



1 **Extreme warming rates affecting alpine areas in SW Europe deduced from algal**

2 **lipids**

3

4 Antonio García-Alix^{1,2,3*}, Jaime L. Toney², Gonzalo Jiménez-Moreno¹, Carmen Pérez-
5 Martínez⁴, Laura Jiménez⁴, Marta Rodrigo-Gámiz¹, R. Scott Anderson⁵, Jon Camuera¹,
6 Francisco J. Jiménez-Espejo³, Dhais Peña-Angulo⁶, María J. Ramos-Román⁷

7

8

9 ¹ Department of Stratigraphy and Paleontology, University of Granada, Granada, 18072,
10 Spain.

11 ² School of Geographical and Earth Sciences, University of Glasgow, Glasgow, G12
12 8QQ, UK.

13 ³ Instituto Andaluz de Ciencias de la Tierra (IACT), CISC-UGR, Armilla, 18100, Spain.

14 ⁴ Department of Ecology and Institute of Water Research, University of Granada,
15 Granada, 18072, Spain.

16 ⁵ School of Earth and Sustainability, Northern Arizona University, Flagstaff, AZ 86011,
17 USA.

18 ⁶ Department of Geography, University of Zaragoza, Zaragoza, 50009 Spain.

19 ⁷ Department of Geosciences and Geography, University of Helsinki, Helsinki, FI-00014,
20 Finland

21

22 * *Correspondence to:* Antonio García-Alix (agalix@ugr.es)

23



24 **Abstract.** Alpine ecosystems of the southern Iberian Peninsula are among the most
25 vulnerable and the first to respond to modern climate change in southwestern Europe.
26 While major environmental shifts have occurred over the last ~1500 years in these alpine
27 environments, only changes in the recent centuries have led to extreme responses, but
28 factors imposing the strongest stress have been unclear until now. To understand these
29 environmental responses, here, for the first time, we calibrated algal lipids (long-chain
30 diols) to instrumental data extending alpine temperatures backward 1500 years. These
31 novel results highlight the enhanced effect of greenhouse gases on alpine temperatures
32 during the last ~200 years and the long-term modulating role of solar forcing. This study
33 also shows that warming rates during the 20th century (~0.18°C/decade) increased ~2.5
34 times with respect to the last stage of the Little Ice Age (~0.07°C/decade), even exceeding
35 temperature trends of the high-altitude Alps during the 20th century. As a consequence,
36 temperature exceeded the pre-industrial threshold in the 1950s, being one of the major
37 forcings of the enhanced recent change in the alpine ecosystems from southern Iberia.
38 Nevertheless, other factors reducing the snow and ice albedo (i.e. atmospheric deposition)
39 may have influenced local glacier loss, since steady climate conditions predominated
40 from middle 19th century to the first decades of the 20th century.

41

42 **1. Introduction**

43

44 Global mean annual surface temperatures have risen by ~0.85°C from 1880 to
45 2012 and the recent decades have been the warmest ones in the Northern Hemisphere
46 during the Common Era (IPCC, 2013). This trend is alarming, since over the last decade
47 temperature records have been broken yearly. For example, in Spain the highest
48 temperatures ever recorded in September and July occurred in 2016 (45.5°C) and 2017



49 (46.9°C-47.3°C), respectively (Spanish National Weather Agency - AEMet Open Data,
50 2019). Increasing global temperatures are contributing not only directly to land and ocean
51 surface warming, but are also changing the global hydrological cycle through the
52 disturbance of atmospheric circulation patterns and moisture (Easterling et al., 2000;
53 IPCC, 2013). As a result, the term “global warming” is migrating towards recent “global
54 change” in order to express the variety of modern climate extremes witnessed across the
55 world. The effects of modern global warming and associated climate change events may
56 be causing extreme environmental impacts, beyond what is recorded in the recent
57 geologic record (Waters et al., 2016). Hence, it is crucial to identify warming thresholds,
58 rates, and forcing mechanisms from past high-resolution temperature records to
59 understand modern climate change. It is especially important in fragile regions such as
60 high elevation ecosystems of southern European mountains. This is the case for the
61 Mediterranean alpine realm, an environmentally vulnerable biodiversity “Hot-Spot”
62 (Schröter et al., 2005;Giorgi, 2006) where recent climate change is affecting species
63 richness and distribution (Pauli et al., 2012;Médail and Quézel, 1999). Therefore, alpine
64 wetlands in the Mediterranean region, such as the ones from the Sierra Nevada in the
65 southern Iberian Peninsula, are sensitive recorders of changing climate and their
66 sedimentological records archive the ecological and biogeochemical responses to
67 different environmental forcings (Catalan et al., 2013).

68

69 In order to contribute to a better understanding of recent climate change events in
70 these vulnerable areas, here, for the first time, we calibrate a recently developed algal-
71 lipid temperature proxy in an alpine lacustrine record that overlaps with instrumental
72 temperature time-series. This calibration allows the reconstruction of temperatures in
73 alpine areas of the southern Iberian Peninsula during the Common Era when instrumental



74 records are discontinuous or non-existent. Temperature-dependent biomarkers, such as
75 those produced by algae (alkenones) or bacteria/archaea (glycerol dialkyl glycerol
76 tetraether: GDGTs) had been commonly used in a wide range of marine records as
77 quantitative paleothermometers, and their further application in lake environments has
78 widely increased in the last decade (i.e., Castañeda and Schouten, 2011; Theroux et al.,
79 2010; Longo et al., 2018; Colcord et al., 2015; Foster et al., 2016). A novel algal-lipid
80 biomarker based on long-chain diols (LCDs), has also been applied as a temperature
81 proxy in marine environments (Rodrigo-Gámiz et al., 2015; Rampen et al., 2012; Rampen
82 et al., 2014b; Rodrigo-Gámiz et al., 2014); however, it has only been used tentatively in
83 freshwater records (Rampen et al., 2014a). In this regard, studies using LCDs as different
84 (paleo)environmental proxies in marine environments (not just only for temperature
85 reconstructions) have increased in the last years, showing the potential of LCDs as
86 upwelling proxies (Versteegh et al., 1997; de Bar et al., 2016), riverine inputs in marine
87 settings (de Bar et al., 2016; Lattaud et al., 2017a), or nutrient proxies (Gal et al., 2018).
88 Nevertheless, only a few studies have applied them for paleoenvironmental
89 reconstructions, such as for paleoproductivity (Shimokawara et al., 2010), past rainfall
90 anomalies (Romero-Viana et al., 2012), or paleotemperatures (Rampen et al., 2014a),
91 among others. In any case, despite the great potential of LCDs for paleoenvironmental
92 reconstructions, there are still a lot of ongoing questions about the applicability of diols
93 at high latitude areas (Rodrigo-Gámiz et al., 2015), in freshwaters records (Rampen et al.,
94 2014a), or even about their biological producers (Villanueva et al., 2014; Balzano et al.,
95 2018).

96

97 The LCD distribution in marine environments shows significant correlations with
98 mean annual sea surface temperature through the ratio of the fractional abundances of C₂₈



99 1,13-diol, C₃₀ 1,13-diol, and C₃₀ 1,15-diol that are used in the Long Chain Diol Index
100 (LDI, Eq. (1)) (Rampen et al., 2012). The use of this index is novel in freshwater
101 environments and only a preliminary calibration with other indirect temperature proxies
102 (i.e., GDGTs) is available (Rampen et al., 2014a). Here, we improve the biomarker
103 paleothermometry by establishing the first temperature calibration for freshwater LCDs
104 using a comparison with historical temperature records for the last ~100 years. These new
105 data support and reinforce the use LCDs as a paleotemperature proxy in freshwater
106 environments.

107

108 Equation (1) $LDI = (F_{C_{30} 1,15\text{-diol}}) / (F_{C_{28} 1,13\text{-diol}} + F_{C_{30} 1,13\text{-diol}} + F_{C_{30} 1,15\text{-diol}})$

109 (Rampen et al., 2012)

110

111 **1.1 Regional settings**

112

113 This paper focuses on the LCD record of two adjacent cores from Laguna de Río
114 Seco (LdRS), a small alpine lake (~0.42 ha and less than 3m of water depth) at 3020 masl
115 in the protected Sierra Nevada National Park, southern Spain (Fig. 1). Alpine Sierra
116 Nevada wetlands, including LdRS, are low primary production (oligo-mesotrophic)
117 systems and their biogeochemical cycles partially depends on aeolian nutrient supplies
118 (i.e. Saharan aerosol deposition), since catchment basins are small and barren in nutrients
119 (Pulido-Villena et al., 2005; Morales-Baquero et al., 2006; Reche et al., 2009).

120

121 Sierra Nevada is the southwestern-most mountain range in Europe, where latest
122 Pleistocene cirque glaciers carved the metamorphic (mica schist) bedrock in the highest
123 peaks (Castillo Martín, 2009). Massive glacier melting at the latest Pleistocene-Holocene



124 transition transformed the former glacial depressions into wetlands (Castillo Martín,
125 2009) that evolved gradually into either shallow lakes or peatlands around the middle-to-
126 late Holocene transition (Jiménez-Espejo et al., 2014;Garcia-Alix et al., 2017). Small
127 glaciers re-appeared at the highest peaks of the Sierra Nevada in the 15th century, during
128 the Little Ice Age, and remained until the 20th century (Oliva et al., 2018). The presence
129 of these glaciers is observed in the sedimentary record in some alpine lakes in the Sierra
130 Nevada (deposit of coarse sediments), like in Laguna de la Mosca (Oliva and Gomez-
131 Ortiz, 2012). However, these kinds of deposits have not been registered in Laguna de Río
132 Seco, where the last 1500 years are characterised by continuous laminated clays and
133 bryophyte layers (Anderson et al., 2011). In any case, glacial effects have not caused any
134 disturbance on wetland sedimentation (i.e., erosion), since local alpine sedimentary
135 records show continuous sedimentation patterns (Anderson et al., 2011;Ramos-Román et
136 al., 2016;García-Alix et al., 2012;Oliva and Gomez-Ortiz, 2012;Mesa-Fernández et al.,
137 2018). During the 20th century this sensitive alpine region of southern Iberia has
138 experienced significant impacts from modern climate change as evidenced, for example,
139 by the first permanent European glacier loss there in the ~1920s (Grunewald and
140 Scheithauer, 2010) and the extreme permafrost reduction during recent decades (Oliva
141 and Gomez-Ortiz, 2012). As a consequence, this glacier and permafrost melting supplied
142 a great amount of water (water availability) (Jiménez et al., 2018a) that boosted the
143 occasional development of local aquatic environments, contrasting with the general
144 environmental aridification trends observed throughout the 20th century (Garcia-Alix et
145 al., 2017;Ramos-Román et al., 2016;Jiménez et al., 2018a).

146

147 The sedimentary archive of LdRS has been selected for this study in order to 1)
148 improve the freshwater LCDs paleothermometry by proposing a new temperature



149 calibration for freshwater LCDs , 2) reconstruct temperatures beyond the instrumental
150 record in a site at the leading edge of changing climate, 3) assess the role of different
151 radiative forcing (i.e., solar radiation or greenhouse gas concentrations) on temperature
152 change in alpine wetlands of the southwestern Europe during the Common Era, and 4)
153 understand the responses to recent climate change in this highly sensitive environment.

154

155 **2. Materials and methods**

156

157 **2.1. Sediment sampling**

158

159 Two sediment cores were taken at the deepest part of LdRS, an alpine lake at 3020
160 masl in the Sierra Nevada (southern Spain) (Fig. 1c). A long sediment core (150 cm) was
161 retrieved in 2006 (LdRS lgc). A short sediment core of 16 cm was collected in 2008
162 (LdRS shc) using a slide-hammer gravity corer (Aquatic Research Instruments, Hope,
163 Idaho, USA). Independent age models were performed in each sediment core to avoid
164 potential correlation problems caused by changes in the sedimentation rates between both
165 coring sites (Fig. 1c) and different sampling dates (2006-LdRS lgc and 2008-LdRS shc).
166 The age model of LdRS lgc is based on ^{210}Pb and ^{137}Cs in the uppermost part (first 15
167 cm), and ^{14}C analyses in older sediments (Anderson et al., 2011). The age model of the
168 LdRS shc is based on gamma spectroscopy by measuring the ^{210}Pb , ^{137}Cs , and ^{226}Ra
169 radionuclides in the first ~14 cm, and afterwards the age was extrapolated to the core
170 bottom (16 cm) (Jiménez et al., 2018b; Jiménez et al., 2018a). Both records show that the
171 sediment accumulation rate for the uppermost 15-16 cm ranges between 0.13 and 0.9
172 cm/yr (Anderson et al., 2011; Jiménez et al., 2018b), and lower sedimentation rates below
173 this depth (~0.008 cm/yr) (Anderson et al., 2011). Ages models show that the LdRS shc



174 extends back to ~200 years with a sample resolution ranging from 5 to 7yr (high-
175 resolution) (Jiménez et al., 2018b; Jiménez et al., 2018a). In the case of the LdRS lgc, the
176 section studied in this paper covers the last ~1500 years with a lower sample resolution.
177 In this case, the sample resolution is around 6-7 years in the first 10 cm, and from 24 to
178 150 years in older samples (Anderson et al., 2011).

179

180 **2.2. Geochemical analyses**

181

182 Thirty-two sediment samples were collected consecutively every 0.5 cm along
183 LdRS shc and twenty samples in the first 22 cm of LdRS lgc. The samples were freeze-
184 dried and homogenized. The total lipid content was extracted from the sediment samples
185 using a Thermo Scientific™ Dionex™ ASE™ 350 Accelerated Solvent Extractor system
186 at 100 °C and 7×10^6 Pa using a mixture of dichloromethane (DCM) and methanol (9:1,
187 v:v). Afterwards, the neutral fraction was separated by means of aminopropyl-silica gel
188 chromatography using DCM:isopropanol (1:1, v:v). This neutral fraction was
189 subsequently eluted with hexane, DCM, ethyl acetate:hexane (25:75, v:v), and methanol
190 through a 230-400 mesh/35-70 micron silica-gel chromatographic column, in order to
191 obtain four neutral sub-fractions (N1-N4). Long chain diols were obtained in the third
192 neutral fraction (N3, alcohol fraction), which was derivatised by bis-(trimethylsilyl)
193 trifluoroacetamide (BSTFA) before running the analyses. 30µL of BSTFA and 40µL of
194 pyridine were added to each N3 fraction and heated at 80 °C for 2 hours. When vials were
195 at room temperature, a volume between 140 µl and 220 µl of DCM was added to each
196 sample. Firstly, the derivatised N3 fractions were analysed with a Gas Chromatography
197 with Flame-Ionization Detector (GC-FID Shimadzu 2010) in order to obtain the proper
198 concentration. Subsequently, they were measured in a Shimadzu QP2010-Plus Mass



199 Spectrometer interfaced with a Shimadzu 2010 GC using a scan mode between m/z 50 –
200 650, in order to obtain a general picture of the mass spectrum of the samples, and on the
201 basis of a Selected-Ion Monitoring mode (SIM), selecting the characteristic fragment ions
202 of the most important long chain diols, i.e. m/z 299, 313, 327, and 341 (Rampen et al.,
203 2012; Versteegh et al., 1997). Fractional abundances of the C_{28} 1,13-diol, C_{30} 1,13-diol,
204 C_{30} 1,15-diol are used in Eq. (1) to calculate the Long chain Diol Index (LDI) (Rampen
205 et al., 2012). Fractional abundances of C_{28} 1,13-diol, C_{30} 1,15-diol, and C_{32} 1,15-diol are
206 used to characterise the potential diol source (i.e. marine, lacustrine, or specific algae
207 groups) (Rampen et al., 2014a; Lattaud et al., 2018).

208

209 **2.3 Reference temperature time-series for LDI temperature calibration**

210

211 Generating an accurate diol-temperature calibration in alpine Sierra Nevada
212 wetlands is challenging, because there is a lack of long and continuous temperature time-
213 series at such high elevations. The meteorological observatories at the Sierra Nevada ski
214 resort (ranging in elevation from 2500 to 3020 masl) only provided discontinuous
215 temperature records from 1965 to 2011 (Spanish National Weather Agency - AEMet Open
216 Data, 2019; Observatorio del cambio global de Sierra Nevada, 2016) that show a
217 significant correlation ($r > 0.95$; $p < 0.0001$) with low elevation temperature time-series
218 (Table S1, S2). This lack of reference temperature time-series in Sierra Nevada alpine
219 areas does not allow the development of a direct LDI-temperature calibration at high-
220 elevation. Therefore, one potential way to obtain a LDI-temperature calibration is by
221 means of the correlation of LDI data with long and reliable historical temperature time-
222 series at nearby lower elevation areas, followed by a correction of the altitudinal effect
223 on temperatures. After testing the correlations between LDI and different low elevation



224 observatories at different scales (mean warm season and mean annual temperatures)
225 (Table S3), we decided to develop the LDI temperature calibrations against the mean
226 annual temperatures from Sevilla-Tablada and Madrid-Retiro observatories, since these
227 are the longest temperature time-series in the region showing the highest correlation with
228 LDI data (see Table S3 for further explanations and Fig. 1a for the location of these low-
229 elevation observatories).

230

231 Two different groups of reference temperature time-series at 3020 masl have been
232 estimated in order to overcome the scarceness of high-elevation temperature time-series
233 in the Sierra Nevada and obtain a reliable mean LDI-temperature calibration: 1) based on
234 the elevational gradient between low and high elevation observatories and 2) based on
235 the direct correlation between temperature time-series from Madrid and Sevilla
236 observatories and that at 3020 masl (Cetursa 5 observatory) in the Sierra Nevada, which
237 is near LdRS and at the same elevation (Table S1).

238

239 Reference temperature time-series 1) The elevational gradient among the
240 reference temperature time-series from Madrid, Sevilla and LdRS is high (there is a
241 difference of more than 2200 m: Table S1); therefore, they cannot be used directly to
242 calibrate the LDI data of LdRS. In order to solve this problem, the environmental lapse
243 rate ($\Delta_{\text{temperature}}/\Delta_{\text{elevation}}$ in °C/m) has been estimated between lower elevation
244 observatories with long temperature time-series (Granada, Sevilla, and Madrid) and those
245 from Sierra Nevada at higher elevation (with shorter temperature time-series: Albergue,
246 and Cetursa 1, 3 and 5) (Table S1). This comparison between low and high elevation
247 observatories show significant correlations ($r>0.95$; $p<0.0001$) (Table S2; Fig. S1). Due
248 to very few annual data points from high elevation sites, monthly and annual (twelve



249 continuous months) environmental lapse rates were calculated to compare both datasets.
250 The calculated temperature shifts between the reference low elevation observatories and
251 LdRS site at 3020 masl, worked out from Fig. S1 equations (Table S4), was applied to
252 the temperature time series from Madrid and Sevilla for the last ~100 years in order to
253 obtain a temperature reconstruction (from 1908 to 2008 CE) at 3020 masl.

254

255 Reference temperature time-series 2) The direct comparison between Madrid and
256 Sevilla temperatures and those from the observatory Cetursa 5 (3020 masl) by means of
257 Ordinary Least Square regressions has given rise to two equations (Fig. S2a and b) that
258 allow the reconstruction of temperature time-series at 3020 masl from 1908 to 2008.

259

260 3. Results

261

262 3.1 Long chain diols in alpine lakes from southern Iberia

263

264 The distribution of the dominant long-chain diol isomers in LdRS (C_{28} , C_{30} and
265 C_{32} 1,13- and 1,15-diols) is different from that of marine and lake sediments as well as of
266 algal cultures and particulate organic matter published up until now (Rampen et al.,
267 2014a; Lattaud et al., 2018) (Fig. 2a). This suggests that diol producers in LdRS are likely
268 different from those identified so far in lacustrine environments and algal culture studies,
269 making the diol puzzle even more complex than originally thought. Eustigmatophyceae
270 algae have been commonly proposed as diol producers in freshwater environments (e.g.
271 *Vischeria* sp., *Eustigmatos* sp.) (Volkman et al., 1999; Rampen et al., 2014a; Villanueva
272 et al., 2014). Nevertheless, in the case of Sierra Nevada wetlands, where planktonic algae
273 communities are very simple (Sánchez-Castillo, 1988), Eustigmatophyceae algae have



274 not been identified so far (Barea-Arco et al., 2001; Sánchez-Castillo, 1988). Conversely,
275 preliminary evidence would point instead to *Chromulina* spp. and/or other planktonic
276 chrysophytes as potential diol producers in this area (Fig. S3). These observations suggest
277 that further work is needed to unravel the real biological source for diols in these alpine
278 wetlands.

279

280 The LDI record obtained from the C₂₈, C₃₀ diols in LdRS depicts important
281 fluctuations during the last ~1500 years, in agreement with the temperature trends during
282 the Common Era. More specifically, LDI values in the long record, LdRS lgc, range from
283 ~0.23 to 0.05 from ~400 to 1900 Common Era years (CE), with the maximum and
284 minimum values at ~930 and ~1690 CE, respectively (Fig. 2b). These changes are coeval
285 with the maximum temperatures of the Medieval Climate Anomaly (MCA) and with the
286 minimum temperatures of the Little Ice Age (LIA). LDI fluctuations were extremely
287 abrupt during the 20th century: from 0.10 to 0.31, according to the lowest resolution record
288 (LdRS lgc) and from 0.13 to 0.32, following the highest resolution record (LdRS shc).
289 These minimum and maximum values were reached in both cases during the first and last
290 decades of the 20th century, respectively (Fig. 2b). As it can be observed, a significant
291 Pearson correlation ($r > 0.7$; $p < 0.004$) exists among the LDI from LdRS shc and global
292 (Hansen et al., 2010) and regional annual instrumental temperatures (Spanish National
293 Weather Agency - AEMet Open Data, 2019) (Table S3, and S5).

294

295 3.2 LDI temperature calibration

296

297 An Ordinary Least Square Regression was run between the two groups of
298 reference temperature time-series at 3020 masl and the LDI record from LdRS shc (Fig.



299 3a). The obtained equation represents the relationship between mean annual temperatures
300 (MAT) and LDI, providing a calibration equation (Eq. (2); Fig. 3a). The residual errors
301 of the obtained temperature calibration, according to both the LDI-reconstructed
302 temperatures and the reference temperature time-series, are lower than 0.8°C, being the
303 standard error 0.26°C. The histogram showing the frequency of the residuals reveals that
304 ~80% of the residuals range from 0.3 to -0.3. Apparently, data from 1973 slightly outlie
305 (residuals ≤ -0.60). This means that the residual errors would be lower than 0.6°C and
306 the standard error ~0.2°C if these outliers were omitted (Fig. 3b).

307

308 Equation (2) $\text{MAT (}^\circ\text{C)} = 9.7028 \times \text{LDI} - 0.37501$ (n=76; $R^2 = 0.81$)

309

310 The application of the obtained calibration to the LDI values of LdRS provides
311 the first temperature reconstruction for the Common Era in this alpine area (Fig. 2c). In
312 order to estimate the real magnitude of temperature variations during this period, the
313 Mean Annual Temperature Anomaly (MATA °C) has been calculated with reference to
314 the mean annual temperatures of the last 30 years of the record (2008-1979). The lowest
315 temperatures were recorded between ~1600 and ~1780 CE, with a temperature anomaly
316 ranging from ~ -2.0 to ~ -2.3 °C. These temperature anomalies only reached positive
317 values after 1998 (Fig. 2c).

318

319 4. Discussion

320

321 4.1 LdRS record in the environmental context of the Iberian Peninsula during the 322 Common Era

323



324 Abrupt changes in temperature and precipitation have been depicted during the
325 last 2000 years in the Iberian Peninsula and surrounding marine areas (Sánchez-López et
326 al., 2016;Moreno et al., 2012). Precipitation was highly variable, showing arid conditions
327 during the MCA, especially in southern Iberia, overall humid conditions throughout the
328 LIA (with a complex internal structure showing large variability in humidity and extreme
329 events), and arid conditions for the Industrial Period (Moreno et al., 2012;Sánchez-López
330 et al., 2016;Oliva et al., 2018;Rodrigo et al., 1999), especially in high elevation wetlands
331 from southern Iberia (Anderson et al., 2011;Jiménez-Espejo et al., 2014;Garcia-Alix et
332 al., 2017).

333

334 As far as reconstructed temperature variations are concerned, although the Early
335 Middle Ages displayed a great temperature variability in the Iberian Peninsula and
336 surrounding marine sites (Sánchez-López et al., 2016;Moreno et al., 2012), three main
337 stages have been identified for the last millennium deduced from different proxies: a
338 warm period throughout the MCA followed by cold temperatures during the LIA, ending
339 in an abrupt warming in the second half of the 20th century (Moreno et al., 2012;Sánchez-
340 López et al., 2016;Oliva et al., 2018). One of the proxies used to reconstruct such
341 temperature variations in continental areas of the Iberian Peninsula were tree ring data.
342 Long tree ring temperature archives of the Iberian Peninsula showed the same overall
343 variations as the ones registered in LdRS, such as high temperatures before 1250 CE
344 (Büntgen et al., 2017), some temperature drops coeval with solar minima during the LIA
345 (i.e. the end of Spörer or Maunder Minima), as well as a period of moderate-low
346 temperatures from ~1850 to ~1940, followed by a temperature increasing trend in the
347 second half of the 20th century with several temperature drops between ~1960 and ~1990
348 (Büntgen et al., 2017; Tejedor et al., 2017). The same trends have been observed in the



349 European summer temperatures deduced from tree ring records (Luterbacher et al., 2016)
350 (Fig. 4b and 5b). Surprisingly, tree ring data from the Pyrenees and Iberian range show
351 minor temperature variations, and even a slight temperature decrease from ~2000 to 2008,
352 which is supported by the LdRS diol record (Fig. 5c). This temperature
353 cooling/stabilization at the beginning of the 21st century is coeval with globally reduced
354 warming rates over the 2001–2014 period (Fyfe et al., 2016).

355

356 Contrasting with these continental temperature reconstructions, high-resolution
357 sea surface temperature (SST) estimations from marine sites surrounding the Iberian
358 Peninsula, such as those derived from alkenones in the Tagus Delta (Iberian Atlantic
359 Margin) or in the Balearic Islands (western Mediterranean Sea), showed a general
360 decreasing trend for the last ~2000 years, with a warm MCA, a cold LIA, and
361 cold/moderate temperatures for the Industrial Period that do not appear to mirror the
362 modern global warming observed throughout the 20th century (Abrantes et al.,
363 2005; Moreno et al., 2012). Only high-resolution alkenone and TEX₈₆ (from GDGTs)
364 derived-SST records of the cores 384B and 436B from the Alboran Sea (Nieto-Moreno
365 et al., 2013) and the alkenone-SST record of core Gol-Ho1B from the Gulf of Lions (Sicre
366 et al., 2016) have shown a clear temperature increase during the 20th century, similar to
367 the LdRS LDI temperature record (Fig. 4a,c, 5a,c). The observed heterogeneity in the
368 SST reconstructions based on biomarkers such as alkenones (Moreno et al.,
369 2012; Abrantes et al., 2005; Rodrigo-Gámiz et al., 2014), GDGTs (Nieto-Moreno et al.,
370 2013) or long chain diols (Rodrigo-Gámiz et al., 2014) could be explained by each record
371 belonging to a different biogeographical area with specific temporal and dynamic
372 oceanographic regimes, and potential dissimilar primary productivity patterns of each
373 algal source (i.e. seasonality or bloom length) (Sicre et al., 2016).



374

375 The previously described climate variability in precipitation and temperature
376 during the last ~1500 years in the Iberian Peninsula have been explained by different
377 forcing mechanisms such as the effect of the westerlies-North Atlantic climate dynamics,
378 internal climate variability, solar irradiance, volcanism, or anthropogenic forcing
379 (Gómez-Navarro et al., 2011;Gómez-Navarro et al., 2012;Moreno et al., 2012;Sánchez-
380 López et al., 2016). Their potential effect on the LDI record from LdRS is discussed in
381 the following section.

382

383 **4.2. Control mechanisms on alpine temperatures in SW Europe during the**

384 **Common Era**

385

386 Solar, volcanic, and anthropogenic (i.e. CO₂ and CH₄) radiative changes, along
387 with the internal variability are usually attributed as the leading factors controlling
388 temperatures during the Common Era (IPCC, 2013;Ammann et al., 2007). In addition,
389 North Atlantic climate dynamics such as the North Atlantic Oscillation (NAO) or the
390 Atlantic Multidecadal Oscillation (AMO) are other potential drivers of natural climate
391 variability in the Iberian Peninsula (O'Reilly et al., 2017;Moreno et al., 2012;Sánchez-
392 López et al., 2016;López-Moreno et al., 2011). The control of the North Atlantic climate
393 dynamics in the studied alpine wetlands is evident, at least for precipitation and humidity
394 fluctuations, since the NAO and solar forcing have been described as the main controls
395 on the paleoenvironmental evolution recorded in this area (Ramos-Román et al.,
396 2016;Garcia-Alix et al., 2017). Conversely, other studies have shown that the NAO
397 climate mode had little effects on temperatures in this alpine area from 1950 to 2006 CE
398 (López-Moreno et al., 2011). LdRS data agree with this observation, since no correlation



399 (Tables S5, S6) has been detected between the NAO reconstruction (Trouet et al., 2009)
400 and the obtained LDI record for the last millennium. In the case of the AMO, it has an
401 impact on the North Atlantic atmospheric blocking mechanisms (Häkkinen et al., 2011)
402 and on the European and Mediterranean temperatures, especially during the AMO warm
403 phases (O'Reilly et al., 2017). In the study area, the AMO shows a moderate long-term
404 correlation (Figs. 4c,d and 5c,d $r>0.60$; $p<0.01$) with both long and short core derived-
405 LDI records, but the correlation decreases when long-term trends are removed ($r<0.32$;
406 $p>0.1$) (Tables S5, S6). Since the nature of the AMO and its specific drivers are still a
407 matter of debate, i.e., internal ocean variability control (multidecadal fluctuations in the
408 Atlantic Meridional Overturning Circulation) versus solar or volcanic forcing for the
409 last centuries (Knudsen et al., 2014), we cannot conclude whether the observed
410 correlations represent the sole effect of the AMO or the influence of its underlying
411 forcing mechanisms.

412

413 The significant correlation at long and short terms ($r>0.61$; $p<0.005$) between
414 LDI-records from LdRS and greenhouse gases (Schmidt et al., 2011) (Fig. 4c,g; Table
415 S6), especially since the beginning of the 20th century (Industrial Period) (Fig. 5c,f; Table
416 S5), suggests that greenhouse gases might have an important effect on temperatures at
417 this high elevation site.

418

419 The potential impact of solar radiation and volcanic eruptions on climate over both
420 short- and long-timescales is a topic of controversy in the literature (Ammann et al.,
421 2007). In this regard, volcanic forcing, which should give rise to negative radiative
422 forcing in the climate system (Ammann et al., 2007; Sigl et al., 2015), do not show a
423 significant correlation with LDI-derived temperatures from LdRS over the last 1500 years



424 (Fig. 4c,g and 5c,h; Table S5, S6). We suggest that this lack of influence at LdRS record
425 is a function of its high-altitude location, at 3020 masl, in the free troposphere, which
426 reduces the environmental impact of small volcanic tropospheric eruptions that likely
427 have greater effects on lower elevation sites (Mather et al., 2013). In addition, the
428 relatively short residence time of volcanic aerosols in the atmosphere mainly causes, at
429 most, decadal-timescale effects (Sigl et al., 2015) that can be difficult to identify in most
430 sedimentary records due to the age resolution, as in the case of older sediments than 200
431 years in LdRS. Nevertheless, large explosive volcanic eruptions delivering large amounts
432 of stratospheric aerosols (Marotzke and Forster, 2015; Sigl et al., 2015), such as that for
433 Agung Volcano in Bali, Indonesia (1963-1964 CE), may be associated with a small
434 depression in LDI-derived temperatures observed in LdRS record (Fig. 5c,g). Although
435 reconstructed-LDI cold temperatures occasionally seem to occur coevally with volcanic
436 eruptions, for example, 560-510 and 320 years ago (~1450-1500 and 1690 CE) (Sigl et
437 al., 2015), there is not a consistent relationship between the intensity and number of large
438 eruptions and the reconstructed coolings in LdRS records, especially over the last ~200
439 years where the age sample resolution would be enough to detect them (LdRS shc).

440

441 Most of the above mentioned cooling events recorded in LdRS, such as those
442 during the LIA, correspond to low solar activity periods like the Spörer Minimum (from
443 ~1450 to 1550 CE) or the Maunder Minimum (from ~1645 to 1715 CE) (Stuiver and
444 Quay, 1980) (Fig. 4 a,b,c,e,f). Thus, long-term correlations between LDI-derived
445 temperatures and solar activity, based on reconstructions of the solar irradiance and
446 cosmogenic isotopes (such as ^{14}C), are evident during the last ~1500 years in LdRS record
447 ($r > 0.69$; $p < 0.002$) (Fig. 4c,e,f; Table S5). This correlation drops ($0.37 < r < 0.56$ and $0.04 <$
448 $p < 0.14$) when long-term trends are removed (Table S6). The long-term solar influence



449 agrees with previous observations in other alpine records of this area (Ramos-Román et
450 al., 2016; Garcia-Alix et al., 2017). Solar activity slightly decreases its long-term
451 influence in LdRS record during the last ~200 years ($r>0.56$; $p<0.001$) and disappears
452 when long-term trends are removed (Table S5). Only some occasional temperature
453 decreases or slower rates of warming such as during the 19th to 20th century transition,
454 from ~1930 to 1940, from ~1960 to 1975, and around 1988 CE, correspond with slight
455 declines in the total solar activity (Fig. 5c,e blue arrows).

456

457 In the same way, LdRS shc registered a small decrease in LDI-derived
458 temperature (or stabilization) at the beginning of the 21st century (Fig. 5c), also recorded
459 in the Madrid and Sevilla temperature time-series (Spanish National Weather Agency -
460 AEMet Open Data, 2019), tree ring records of the the Pyrenees and Iberian Range
461 (Tejedor et al., 2017; Büntgen et al., 2017), in marine platforms of the western
462 Mediterranean (Fig. 5a) (Sicre et al., 2016) or globally (Fyfe et al., 2016). Although this
463 slowdown agrees with a decreasing trend in solar activity and a slight stabilization of
464 atmospheric methane concentrations, the causes are more complex, and probably related
465 to a combination of internal variability and radiative forcing (i.e. volcanic and solar
466 activity, or decadal timescale changes in anthropogenic aerosols) (Fyfe et al., 2016).

467

468 **4.3. Exceeding natural thresholds in alpine areas**

469

470 The LDI-derived temperature reconstructions from LdRS show that in the early
471 1950s temperature exceeded for the first time the highest temperature values reached in
472 the record during the MCA (Fig. 4c). Although this means that the local temperature
473 natural threshold was surpassed, the low sample density during the MCA precludes



474 setting a robust turning point. In any case, temperature values increased by ~ 1.2 °C in this
475 alpine area after ~ 1950 CE, under full anthropogenic influence. The comparison between
476 pre-industrial and post-industrial scenarios in the study site highlights the human impact
477 on natural trends. The temperature increase during the last stages of the LIA (from ~ 1690
478 to ~ 1850 CE), an analogue for a non-anthropogenic temperature-increase scenario, was
479 ~ 1.2 °C (~ 0.07 °C/decade; Fig. 6), whereas the mean temperature rise throughout the 20th
480 century was ~ 1.8 °C (~ 0.18 °C/decade; Fig. 6). Although this means that on average, the
481 warming rate was 2.5 times faster throughout the 20th century than at the end of the LIA
482 (Fig. 6), these observations are based on a low sample density for the LIA, which might
483 slightly increase the uncertainty for this period. By comparison, average global
484 temperatures rose by ~ 0.85 °C from 1880 to 2012 CE, corresponding to 0.06 °C/decade
485 (IPCC, 2013), which highlight the high-elevation amplification effect of temperatures on
486 this vulnerable area.

487

488 An even more alarming result is that other European alpine areas in the
489 Mediterranean region, such as those from the Alps, experienced a slower warming rate
490 during the 20th century (~ 0.11 °C/decade) (Fig. 6) (Auer et al., 2007; Böhm et al., 2010).
491 This is ~ 1.6 times slower than the warming rate recorded in the Sierra Nevada. This
492 evidence, along with the generally smaller amount of precipitation in the alpine areas of
493 the western Mediterranean region (Auer et al., 2007; Rodrigo et al., 1999), allows us to
494 conclude that the 20th century environmental stress in this area was greater than in the
495 Alps.

496

497 Future scenarios are not optimistic for Sierra Nevada alpine areas either as
498 projected temperature may rise at least ~ 1.4 °C by the end of the 21st century (Fig. 7c).



499 This means that MAT at ~3020 masl would increase to ~4 °C, which is more than 1.5
500 times higher than present mean temperatures (°C). This projection exceeds the ones from
501 the CMIP5 models discussed in the IPCC-2013 report for the end of the 21st century under
502 a low emission scenario (RCP2.6). It is closer to the average temperature increase under
503 the medium-low emission scenario (RCP4.5), and in the low range of a medium-high
504 emission scenario (RCP6.0) (IPCC, 2013). The projected temperature increase in Sierra
505 Nevada would give rise to abrupt and foreseeable environmental consequences such as
506 an evapotranspiration increase and a dramatic reduction in the snow cover. This would
507 consequently amplify the observed decrease in water availability in this semiarid alpine
508 area during the 20th century (Garcia-Alix et al., 2017; Jiménez et al., 2018b) and thus,
509 affecting the water reservoirs for the human population at lower elevations. This scenario
510 would impact on more than 500,000 people in the city of Granada and neighbouring
511 towns, on more than 20,000 ha of irrigated agriculture in southwestern Spain, and would
512 reduce the hydroelectricity production in this area. This would have a more significant
513 impact locally in Sierra Nevada, where endemic and endangered species inhabit
514 (Munguira and Martin, 1993; Blanca, 2001). The projected warming would amplify the
515 gradual reduction in alpine wetland areas that has been observed during the last millennia
516 as a consequence of long-term natural variations along with the superimposed effect of
517 the human-induced environmental change (Garcia-Alix et al., 2017). Alpine wetlands in
518 the southern Iberian Peninsula might disappear under this scenario, resulting in an
519 environmental crisis.

520

521 **4.4. Impact on the southwesternmost European alpine glaciers**

522



523 The studied alpine area supported the southernmost glaciers in Europe during the
524 LIA. Glaciers and permanent snow fields below ~3000 masl, such as those of Corral del
525 Mulhacen (~2950 masl) whose last mention in the literature was between 1809 and 1849
526 CE (Oliva and Gomez-Ortiz, 2012), would have totally disappeared by the decrease in
527 regional precipitation at the beginning of the 19th century (Rodrigo et al., 1999). The
528 climatic features at the end of the 19th century and the beginning of the 20th century did
529 not allow this glacier to re-establish itself (Fig. 7). Post-LIA climatic conditions have also
530 been proposed as the trigger for the melting of the Corral del Veleta Glacier in Sierra
531 Nevada (~3100 masl) at the beginning of the 20th century (Garcia-Alix et al., 2017;Oliva
532 and Gomez-Ortiz, 2012;Oliva et al., 2018). However, our new temperature record show
533 that temperatures did not exceed the levels of the 1850s until the late 1940s CE.
534 Precipitation was low in the southern Iberian Peninsula during the first half of the 20th
535 century, but similar, and even lower, precipitation values were registered before ~1850
536 CE (Rodrigo et al., 1999;Spanish National Weather Agency - AEMet Open Data, 2019)
537 (Fig. 7). Therefore, how could the glacier have retreated under this almost steady-state
538 scenario? A similar paradox has been described in the Alps (Painter et al., 2013), where
539 glaciers began to sharply retreat after the mid-19th century, even though temperature and
540 precipitation records would suggest that glacier expansion should have occurred at least
541 until the first decades of the 20th century. In this case the trigger of the glacial retreat was
542 the industrial black carbon deposition that amplified the solar radiation absorbed at the
543 snow surface and caused its subsequent melting - not a temperature or precipitation
544 change (Painter et al., 2013). Our data suggest that temperature and precipitation were
545 not the only drivers of glacial retreat that led to the melting of permanent glaciers in the
546 Sierra Nevada in the 1920s. Instead, mirroring the case of the Alps, it is plausible that
547 other factors reducing the albedo, such as enhanced atmospheric deposition may have



548 played a strong role. In this regard, important atmospheric depositional events have been
549 recorded in the study alpine sites of southern Iberia from the mid-19th century to the first
550 decades of the 20th century caused by both enhanced North African dust fluxes (Mulitza
551 et al., 2010) (Jiménez et al., 2018b) as well as a spike in atmospheric pollution (as
552 observed in anthropogenic Pb and Hg records in Sierra Nevada; Fig. 7) (Garcia-Alix et
553 al., 2017; Garcia-Alix et al., 2013). Similarly, both phenomena have been demonstrated
554 as triggers for glacier retreat (Painter et al., 2013) and snow melt in the Alps (Di Mauro
555 et al., 2018).

556

557 Melting of the last glaciated area in the Sierra Nevada during the first decades of
558 the 20st century (Grunewald and Scheithauer, 2010) represents an important turning point
559 regarding recent environmental change in this alpine region (Garcia-Alix et al.,
560 2017; Jiménez et al., 2018a). The rapid pace of environmental change in the area after this
561 date is attributed to an amplified effect of warming and aridification (Fig. 7b,c) that
562 increased stress on vulnerable ecosystems (Garcia-Alix et al., 2017; Jiménez et al.,
563 2018b; Jiménez et al., 2018a) with little hope for return of local glaciers.

564

565 **5. Concluding remarks**

566

567 This study shows the vulnerability of alpine regions and the importance of their
568 monitoring for a better understanding of climate variability and future rapid responses. In
569 this regard, algal-derived biomarkers from LdRS records have given rise to the first long-
570 chain diol temperature calibration in freshwater environments by means of the
571 comparison with instrumental temperature data. The combination of a short and long
572 sediment core has provided both a highly accurate LDI-temperature calibration for the



573 instrumental period and a long-term historical perspective on the modern warming. This
574 approach delivers a better time-integrated temperature model than discrete temperature
575 measurements for the 20th century.

576

577 The low sample resolution in the longer core before~1500 CE does not allow us
578 to totally constrain the main natural controls on temperatures in this high-elevation site
579 for the whole Common Era. However, the general trends support that the presumed
580 primary effect of greenhouse gases on temperatures reconstructed from algal-lipids in this
581 alpine region of southern Iberia is likely modulated by long-term solar forcing. In recent
582 times, greenhouse gases seem to be the major temperature driver in this high elevation
583 site. Volcanic forcing appears to have little effect on reconstructed temperatures in this
584 alpine area. The Atlantic Multidecadal Oscillation (AMO) have also shown to have a
585 long-term effect in the study area; however, due its complex nature, the real effect of
586 the AMO on reconstructed temperatures in LdRS cannot be fully constrained. In any
587 case, the effect of the internal climate variability on local temperatures cannot be ruled
588 out. LdRS record also highlights the potential impact that non-climatic environmental
589 drivers such as atmospheric dust and pollution deposition can have exerted on these
590 remote alpine environments (i.e. glacier melting).

591

592 Alpine temperatures of southern Iberia abruptly increased in the 1950s, exceeding
593 the highest temperature scores reached in pre-industrial times. This means that the rate of
594 warming throughout the 20th century increased ~2.5 times compared to the rate in the last
595 stages of the LIA. Furthermore, this modern warming rate is even higher in the Sierra
596 Nevada than in the Alps, pointing towards more environmental stress in these ecosystems.
597 In addition to the amplified effect of warming and aridification, the local environmental



598 pressure may have enhanced throughout the 20th century due to the disappearance of
599 perennial snow fields and the gradual reduction of the seasonal snow cover affecting the
600 local water availability. All these evidences in this fragile alpine region point towards an
601 even worse scenario by the end of the 21st.

602

603 **Data availability.** Fractional abundances of the C₂₈ 1,13-diol, C₃₀ 1,13-diol, C₃₀ 1,15-
604 diol, and C₃₂ 1,15-diol from both studied cores (LdRS shc and LdRS lgc) are available
605 in Table S7.

606

607 **Supplement.** The supplement related to this article is available online at:

608 <https://doi.org/>

609

610 **Author contributions.** The study was conceived by AG-A and JLT. CPM, LJ, GJM,
611 and RSA recovered the sediment cores. AG-A analysed the samples and processed the
612 data. All co-authors discussed the data and equally contributed to the preparation of the
613 manuscript.

614

615 **Competing interests.** The authors declare that they have no conflict of interest.

616

617 **Acknowledgements.** We would like to thank to V. Slaymark (University of Glasgow),
618 for her help preparing and analysing the organic and inorganic samples, as well as F.J.
619 Bonet García and C. González Hidalgo for providing the temperature time-series from
620 Sierra Nevada and south of Spain, respectively.

621

622 **Financial support.** This study was supported by the project P11-RNM 7332 of the “Junta



623 de Andalucía”, the projects CGL2017-85415-R, CGL2013-47038-R and CGL2011-
624 23483 of the “Ministerio de Economía y Competitividad of Spain and Fondo Europeo de
625 Desarrollo Regional FEDER”, the project 87/2007 of the OAPN-Ministerio de Medio
626 Ambiente, as well as the research group RNM-190 (Junta de Andalucía). A.G.-A. was
627 also supported by a Marie Curie Intra-European Fellowship of the 7th Framework
628 Programme for Research, Technological Development and Demonstration of the
629 European Commission (NAOSIPUK. Grant Number: PIEF-GA-2012-623027) and by a
630 Ramón y Cajal Fellowship RYC-2015-18966 of the Spanish Government (Ministerio de
631 Economía y Competitividad). J.L.T. hosted the NAOSIPUK project (PIEF-GA-2012-
632 623027) at the University of Glasgow.

633

634 **References**

635

- 636 Abrantes, F., Lebreiro, S., Rodrigues, T., Gil, I., Bartels-Jónsdóttir, H., Oliveira, P.,
637 Kissel, C., and Grimalt, J. O.: Shallow-marine sediment cores record climate
638 variability and earthquake activity off Lisbon (Portugal) for the last 2000 years,
639 *Quaternary Science Reviews*, 24, 2477-2494,
640 <https://doi.org/10.1016/j.quascirev.2004.04.009>, 2005.
- 641 Ammann, C. M., Joos, F., Schimel, D. S., Otto-Bliesner, B. L., and Tomas, R. A.: Solar
642 influence on climate during the past millennium: Results from transient simulations
643 with the NCAR Climate System Model, *Proceedings of the National Academy of
644 Sciences*, 104, 3713-3718, [10.1073/pnas.0605064103](https://doi.org/10.1073/pnas.0605064103), 2007.
- 645 Anderson, R. S., Jiménez-Moreno, G., Carrión, J., and Pérez-Martínez, C.: Postglacial
646 history of alpine vegetation, fire, and climate from Laguna de Río Seco, Sierra Nevada,
647 southern Spain, *Quaternary Science Reviews*, 30, 1615–1629, 2011.
- 648 Auer, I., Böhm, R., Jurkovic, A., Lipa, W., Orlik, A., Potzmann, R., Schöner, W.,
649 Ungersböck, M., Matulla, C., Briffa, K., Jones, P., Efthymiadis, D., Brunetti, M.,
650 Nanni, T., Maugeri, M., Mercalli, L., Mestre, O., Moisselin, J.-M., Begert, M., Müller-
651 Westermeier, G., Kveton, V., Bochnicek, O., Stastny, P., Lapin, M., Szalai, S.,



- 652 Szentimrey, T., Cegnar, T., Dolinar, M., Gajic-Capka, M., Zaninovic, K., Majstorovic,
653 Z., and Nieplova, E.: HISTALP—historical instrumental climatological surface time
654 series of the Greater Alpine Region, *International Journal of Climatology*, 27, 17-46,
655 10.1002/joc.1377, 2007.
- 656 Barea-Arco, J., Pérez-Martínez, C., and Morales-Baquero, R.: Evidence of a mutualistic
657 relationship between an algal epibiont and its host, *Daphnia pulex*, *Limnology and*
658 *Oceanography*, 46, 871-881, 2001.
- 659 Blanca, G.: *Flora amenazada y endémica de Sierra Nevada*, Consejería de Medio
660 Ambiente de la Junta de Andalucía and University of Granada, 2001.
- 661 Böhm, R., Jones, P. D., Hiebl, J., Frank, D., Brunetti, M., and Maugeri, M.: The early
662 instrumental warm-bias: a solution for long central European temperature series 1760–
663 2007, *Climatic Change*, 101, 41-67, 10.1007/s10584-009-9649-4, 2010.
- 664 Büntgen, U., Krusic, P. J., Verstege, A., Sangüesa-Barreda, G., Wagner, S., Camarero, J.
665 J., Ljungqvist, F. C., Zorita, E., Oppenheimer, C., Konter, O., Tegel, W., Gärtner, H.,
666 Cherubini, P., Reinig, F., and Esper, J.: New Tree-Ring Evidence from the Pyrenees
667 Reveals Western Mediterranean Climate Variability since Medieval Times, *Journal of*
668 *Climate*, 30, 5295-5318, 10.1175/jcli-d-16-0526.1, 2017.
- 669 Castañeda, I. S., and Schouten, S.: A review of molecular organic proxies for examining
670 modern and ancient lacustrine environments, *Quaternary Science Reviews*, 30, 2851-
671 2891, <http://dx.doi.org/10.1016/j.quascirev.2011.07.009>, 2011.
- 672 Castillo Martín, A.: *Lagunas de Sierra Nevada*, Editorial Universidad de Granada,
673 Granada, 2009.
- 674 Catalan, J., Pla-Rabés, S., Wolfe, A. P., Smol, J. P., Rühland, K. M., Anderson, N. J.,
675 Kopáček, J., Stuchlík, E., Schmidt, R., Koinig, K. A., Camarero, L., Flower, R. J.,
676 Heiri, O., Kamenik, C., Korhola, A., Leavitt, P. R., Psenner, R., and Renberg, I.:
677 Global change revealed by palaeolimnological records from remote lakes: a review,
678 *Journal of Paleolimnology*, 49, 513-535, 10.1007/s10933-013-9681-2, 2013.
- 679 Coddington, O., Lean, J. L., Pilewskie, P., Snow, M., and Lindholm, D.: A Solar
680 Irradiance Climate Data Record, *Bulletin of the American Meteorological Society*, 97,
681 1265-1282, 10.1175/bams-d-14-00265.1, 2016.
- 682 Colcord, D. E., Cadieux, S. B., Brassell, S. C., Castañeda, I. S., Pratt, L. M., and White,
683 J. R.: Assessment of branched GDGTs as temperature proxies in sedimentary records
684 from several small lakes in southwestern Greenland, *Organic Geochemistry*, 82, 33-
685 41, <https://doi.org/10.1016/j.orggeochem.2015.02.005>, 2015.



- 686 de Bar, M. W., Dorhout, D. J. C., Hopmans, E. C., Rampen, S. W., Sinnighe Damsté, J.
687 S., and Schouten, S.: Constraints on the application of long chain diol proxies in the
688 Iberian Atlantic margin, *Organic Geochemistry*, 101, 184-195,
689 <https://doi.org/10.1016/j.orggeochem.2016.09.005>, 2016.
- 690 Di Mauro, B., Garzonio, R., Rossini, M., Filippa, G., Pogliotti, P., Galvagno, M., Morra
691 di Cella, U., Migliavacca, M., Baccolo, G., Clemenza, M., Delmonte, B., Maggi, V.,
692 Dumont, M., Tuzet, F., Lafaysse, M., Morin, S., Cremonese, E., and Colombo, R.:
693 Saharan dust events in the European Alps: role on snowmelt and geochemical
694 characterization, *The Cryosphere Discuss.*, 2018, 1-28, 10.5194/tc-2018-241, 2018.
- 695 Easterling, D. R., Meehl, G. A., Parmesan, C., Changnon, S. A., Karl, T. R., and Mearns,
696 L. O.: Climate Extremes: Observations, Modeling, and Impacts, *Science*, 289, 2068-
697 2074, 2000.
- 698 Foster, L. C., Pearson, E. J., Juggins, S., Hodgson, D. A., Saunders, K. M., Verleyen, E.,
699 and Roberts, S. J.: Development of a regional glycerol dialkyl glycerol tetraether
700 (GDGT)-temperature calibration for Antarctic and sub-Antarctic lakes, *Earth and
701 Planetary Science Letters*, 433, 370-379, <https://doi.org/10.1016/j.epsl.2015.11.018>,
702 2016.
- 703 Fyfe, J. C., Meehl, G. A., England, M. H., Mann, M. E., Santer, B. D., Flato, G. M.,
704 Hawkins, E., Gillett, N. P., Xie, S.-P., Kosaka, Y., and Swart, N. C.: Making sense of
705 the early-2000s warming slowdown, *Nature Climate Change*, 6, 224,
706 [10.1038/nclimate2938](https://doi.org/10.1038/nclimate2938), 2016.
- 707 Gal, J.-K., Kim, J.-H., and Shin, K.-H.: Distribution of long chain alkyl diols along a
708 south-north transect of the northwestern Pacific region: Insights into a paleo sea
709 surface nutrient proxy, *Organic Geochemistry*, 119, 80-90,
710 <https://doi.org/10.1016/j.orggeochem.2018.01.010>, 2018.
- 711 Garcia-Alix, A., Jimenez-Espejo, F. J., Lozano, J. A., Jimenez-Moreno, G., Martinez-
712 Ruiz, F., Garcia Sanjuan, L., Aranda Jimenez, G., Garcia Alfonso, E., Ruiz-Puertas,
713 G., and Anderson, R. S.: Anthropogenic impact and lead pollution throughout the
714 Holocene in Southern Iberia, *Science of the Total Environment*, 449, 451-460,
715 <https://doi.org/10.1016/j.scitotenv.2013.01.081>, 2013.
- 716 Garcia-Alix, A., Jimenez Espejo, F. J., Toney, J. L., Jiménez-Moreno, G., Ramos-Román,
717 M. J., Anderson, R. S., Ruano, P., Queralt, I., Delgado Huertas, A., and Kuroda, J.:
718 Alpine bogs of southern Spain show human-induced environmental change



- 719 superimposed on long-term natural variations, *Scientific Reports*, 7, 7439
720 <https://doi.org/10.1038/s41598-017-07854-w>, 2017.
- 721 García-Alix, A., Jiménez-Moreno, G., Anderson, R. S., Jiménez Espejo, F. J., and
722 Delgado Huertas, A.: Holocene environmental change in southern Spain deduced from
723 the isotopic record of a high-elevation wetland in Sierra Nevada, *Journal of*
724 *Paleolimnology*, 48, 471-484, <https://doi.org/10.1007/s10933-012-9625-2>, 2012.
- 725 Giorgi, F.: Climate change hot-spots, *Geophysical Research Letters*, 33,
726 10.1029/2006GL025734, 2006.
- 727 Gómez-Navarro, J. J., Montávez, J. P., Jerez, S., Jiménez-Guerrero, P., Lorente-Plazas,
728 R., González-Rouco, J. F., and Zorita, E.: A regional climate simulation over the
729 Iberian Peninsula for the last millennium, *Clim. Past*, 7, 451-472, 10.5194/cp-7-451-
730 2011, 2011.
- 731 Gómez-Navarro, J. J., Montávez, J. P., Jiménez-Guerrero, P., Jerez, S., Lorente-Plazas,
732 R., González-Rouco, J. F., and Zorita, E.: Internal and external variability in regional
733 simulations of the Iberian Peninsula climate over the last millennium, *Clim. Past*, 8,
734 25-36, 10.5194/cp-8-25-2012, 2012.
- 735 Gonzalez-Hidalgo, J. C., Peña-Angulo, D., Brunetti, M., and Cortesi, N.: MOTEDAS: a
736 new monthly temperature database for mainland Spain and the trend in temperature
737 (1951–2010), *International Journal of Climatology*, 35, 4444-4463, 10.1002/joc.4298,
738 2015.
- 739 Grunewald, K., and Scheithauer, J.: Europe's southernmost glaciers: response and
740 adaptation to climate change, *Journal of Glaciology*, 56, 129-142, 2010.
- 741 Häkkinen, S., Rhines, P. B., and Worthen, D. L.: Atmospheric Blocking and Atlantic
742 Multidecadal Ocean Variability, *Science*, 334, 655-659, 10.1126/science.1205683,
743 2011.
- 744 Hansen, J., Ruedy, R., Sato, M., and Lo, K.: Global Surface Temperature Change,
745 *Reviews of Geophysics*, 48, 10.1029/2010RG000345, 2010.
- 746 IPCC: Climate Change 2013: The Physical Science Basis. Contribution of Working
747 Group I to the Fifth Assessment Report of the Intergovernmental Panel on Climate
748 Change, Cambridge University Press, Cambridge, United Kingdom and New York,
749 NY, USA, 1535 pp., 2013.
- 750 IPCC: Climate Change 2013: The Physical Science Basis. Contribution of Working
751 Group I to the Fifth Assessment Report of the Intergovernmental Panel on Climate



- 752 Change, Cambridge University Press, Cambridge, United Kingdom and New York,
753 USA, 2013.
- 754 Jiménez, L., Conde-Porcuna, J. M., García-Alix, A., Toney, J. L., Anderson, R. S., Heiri,
755 O., and Pérez-Martínez, C.: Ecosystem Responses to Climate-Related Changes in a
756 Mediterranean Alpine Environment Over the Last ~180 Years, *Ecosystems*,
757 10.1007/s10021-018-0286-5, 2018a.
- 758 Jiménez, L., Rühland, K. M., Jeziorski, A., Smol, J. P., and Pérez-Martínez, C.: Climate
759 change and Saharan dust drive recent cladoceran and primary production changes in
760 remote alpine lakes of Sierra Nevada, Spain, *Global Change Biology*, 28, e139–e158,
761 <https://doi.org/10.1111/gcb.13878>, 2018b.
- 762 Jiménez-Espejo, F. J., García-Alix, A., Jiménez-Moreno, G., Rodrigo-Gámiz, M.,
763 Anderson, R. S., Rodríguez-Tovar, F. J., Martínez-Ruiz, F., Giralt, S., Delgado
764 Huertas, A., and Pardo-Igúzquiza, E.: Saharan aeolian input and effective humidity
765 variations over western Europe during the Holocene from a high altitude record,
766 *Chemical Geology*, 374-375, 1-12, <https://doi.org/10.1016/j.chemgeo.2014.03.001>,
767 2014.
- 768 Knudsen, M. F., Jacobsen, B. H., Seidenkrantz, M.-S., and Olsen, J.: Evidence for
769 external forcing of the Atlantic Multidecadal Oscillation since termination of the Little
770 Ice Age, *Nature Communications*, 5, 3323, 10.1038/ncomms4323, 2014.
- 771 Lattaud, J., Dorhout, D., Schulz, H., Castañeda, I. S., Schefuß, E., Sinninghe Damsté, J.
772 S., and Schouten, S.: The C32 alkane-1,15-diol as a proxy of late Quaternary riverine
773 input in coastal margins, *Clim. Past*, 13, 1049-1061, 10.5194/cp-13-1049-2017, 2017a.
- 774 Lattaud, J., Kim, J.-H., De Jonge, C., Zell, C., Sinninghe Damsté, J. S., and Schouten, S.:
775 The C32 alkane-1,15-diol as a tracer for riverine input in coastal seas, *Geochimica et*
776 *Cosmochimica Acta*, 202, 146-158, <https://doi.org/10.1016/j.gca.2016.12.030>, 2017b.
- 777 Lattaud, J., Kirkels, F., Peterse, F., Freymond, C. V., Eglinton, T. I., Hefter, J.,
778 Mollenhauer, G., Balzano, S., Villanueva, L., van der Meer, M. T. J., Hopmans, E. C.,
779 Sinninghe Damsté, J. S., and Schouten, S.: Long-chain diols in rivers: distribution and
780 potential biological sources, *Biogeosciences*, 15, 4147-4161, 10.5194/bg-15-4147-
781 2018, 2018.
- 782 Longo, W. M., Huang, Y., Yao, Y., Zhao, J., Giblin, A. E., Wang, X., Zech, R.,
783 Haberzettl, T., Jardillier, L., Toney, J., Liu, Z., Krivonogov, S., Kolpakova, M., Chu,
784 G., D'Andrea, W. J., Harada, N., Nagashima, K., Sato, M., Yonenobu, H., Yamada,
785 K., Gotanda, K., and Shinozuka, Y.: Widespread occurrence of distinct alkenones from



- 786 Group I haptophytes in freshwater lakes: Implications for paleotemperature and
787 paleoenvironmental reconstructions, *Earth and Planetary Science Letters*, 492, 239-
788 250, <https://doi.org/10.1016/j.epsl.2018.04.002>, 2018.
- 789 López-Moreno, J. I., Vicente-Serrano, S. M., Morán-Tejeda, E., Lorenzo-Lacruz, J.,
790 Kenawy, A., and Beniston, M.: Effects of the North Atlantic Oscillation (NAO) on
791 combined temperature and precipitation winter modes in the Mediterranean
792 mountains: Observed relationships and projections for the 21st century, *Global and
793 Planetary Change*, 77, 62-76, <http://dx.doi.org/10.1016/j.gloplacha.2011.03.003>,
794 2011.
- 795 Luterbacher, J., Werner, J. P., Smerdon, J. E., Fernández-Donado, L., González-Rouco,
796 F. J., Barriopedro, D., Ljungqvist, F. C., Büntgen, U., Zorita, E., Wagner, S., Esper, J.,
797 McCarroll, D., Toreti, A., Frank, D., Jungclaus, J. H., Barriendos, M., Bertolin, C.,
798 Bothe, O., Brázdil, R., Camuffo, D., Dobrovolný, P., Gagen, M., García-Bustamante,
799 E., Ge, Q., Gómez-Navarro, J. J., Guiot, J., Hao, Z., Hegerl, G. C., Holmgren, K.,
800 Klimenko, V. V., Martín-Chivelet, J., Pfister, C., Roberts, N., Schindler, A., Schurer,
801 A., Solomina, O., von Gunten, L., Wahl, E., Wanner, H., Wetter, O., Xoplaki, E.,
802 Yuan, N., Zanchettin, D., Zhang, H., and Zerefos, C.: European summer temperatures
803 since Roman times, *Environmental Research Letters*, 11, 024001, [citeulike-article-
804 id:14089240](https://doi.org/10.1088/1748-9326/11/2/024001)
805 doi: 10.1088/1748-9326/11/2/024001, 2016.
- 806 Mann, M. E., Zhang, Z., Rutherford, S., Bradley, R. S., Hughes, M. K., Shindell, D.,
807 Ammann, C., Faluvegi, G., and Ni, F.: Global Signatures and Dynamical Origins of
808 the Little Ice Age and Medieval Climate Anomaly, *Science*, 326, 1256-1260,
809 [10.1126/science.1177303](https://doi.org/10.1126/science.1177303), 2009.
- 810 Marotzke, J., and Forster, P. M.: Forcing, feedback and internal variability in global
811 temperature trends, *Nature*, 517, 565-570, [10.1038/nature14117](https://doi.org/10.1038/nature14117), 2015.
- 812 Mather, T. A., Pyle, D. M., and Oppenheimer, C.: Tropospheric Volcanic Aerosol, in:
813 *Volcanism and the Earth's Atmosphere*, American Geophysical Union, 189-212, 2013.
- 814 Médail, F., and Quézel, P.: Biodiversity Hotspots in the Mediterranean Basin: Setting
815 Global Conservation Priorities, *Conservation Biology*, 13, 1510-1513,
816 [10.1046/j.1523-1739.1999.98467.x](https://doi.org/10.1046/j.1523-1739.1999.98467.x), 1999.
- 817 Mesa-Fernández, J. M., Jiménez-Moreno, G., Rodrigo-Gámiz, M., García-Alix, A.,
818 Jiménez-Espejo, F. J., Martínez-Ruiz, F., Anderson, R. S., Camuera, J., and Ramos-
819 Román, M. J.: Vegetation and geochemical responses to Holocene rapid climate



- 820 change in the Sierra Nevada (southeastern Iberia): the Laguna Hondera record, *Clim.*
821 *Past*, 14, 1687-1706, 10.5194/cp-14-1687-2018, 2018.
- 822 Morales-Baquero, R., Pulido-Villena, E., and Reche, I.: Atmospheric inputs of
823 phosphorus and nitrogen to the southwest Mediterranean region: Biogeochemical
824 responses of high mountain lakes, *Limnology and Oceanography* 51, 830–837, 2006.
- 825 Moreno, A., Pérez, A., Frigola, J., Nieto-Moreno, V., Rodrigo-Gámiz, M., Martrat, B.,
826 González-Sampériz, P., Morellón, M., Martín-Puertas, C., Corella, J. P., Belmonte, Á.,
827 Sancho, C., Cacho, I., Herrera, G., Canals, M., Grimalt, J. O., Jiménez-Espejo, F.,
828 Martínez-Ruiz, F., Vegas-Vilarrúbia, T., and Valero-Garcés, B. L.: The Medieval
829 Climate Anomaly in the Iberian Peninsula reconstructed from marine and lake records,
830 *Quaternary Science Reviews*, 43, 16-32, 10.1016/j.quascirev.2012.04.007, 2012.
- 831 Mulitza, S., Heslop, D., Pittauerova, D., Fischer, H. W., Meyer, I., Stuut, J.-B., Zabel, M.,
832 Mollenhauer, G., Collins, J. A., Kuhnert, H., and Schulz, M.: Increase in African dust
833 flux at the onset of commercial agriculture in the Sahel region, *Nature*, 466, 226-228,
834 [http://www.nature.com/nature/journal/v466/n7303/abs/nature09213.html#supplemen](http://www.nature.com/nature/journal/v466/n7303/abs/nature09213.html#supplementary-information)
835 [tary-information](http://www.nature.com/nature/journal/v466/n7303/abs/nature09213.html#supplementary-information), 2010.
- 836 Munguira, M. L., and Martin, J.: The Sierra Nevada blue, *Polyommatus golgus* (Hiibner),
837 in: *Conservation Biology of Lycaenidae (Butterflies)*, edited by: New, T. R., IUCN,
838 Gland, Switzerland, 1993.
- 839 Nieto-Moreno, V., Martínez-Ruiz, F., Willmott, V., García-Orellana, J., Masqué, P., and
840 Sinninghe Damsté, J. S.: Climate conditions in the westernmost Mediterranean over
841 the last two millennia: An integrated biomarker approach, *Organic Geochemistry*, 55,
842 1-10, <https://doi.org/10.1016/j.orggeochem.2012.11.001>, 2013.
- 843 O'Reilly, C. H., Woollings, T., and Zanna, L.: The Dynamical Influence of the Atlantic
844 Multidecadal Oscillation on Continental Climate, *Journal of Climate*, 30, 7213-7230,
845 10.1175/jcli-d-16-0345.1, 2017.
- 846 Oliva, M., and Gomez-Ortiz, A.: Late-Holocene environmental dynamics and climate
847 variability in a Mediterranean high mountain environment (Sierra Nevada, Spain)
848 inferred from lake sediments and historical sources, *The Holocene*, 22, 915-927,
849 <https://doi.org/10.1177/0959683611434235>, 2012.
- 850 Oliva, M., Ruiz-Fernández, J., Barriendos, M., Benito, G., Cuadrat, J. M., Domínguez-
851 Castro, F., García-Ruiz, J. M., Giralt, S., Gómez-Ortiz, A., Hernández, A., López-
852 Costas, O., López-Moreno, J. I., López-Sáez, J. A., Martínez-Cortizas, A., Moreno,
853 A., Prohom, M., Saz, M. A., Serrano, E., Tejedor, E., Trigo, R., Valero-Garcés, B.,



- 854 and Vicente-Serrano, S. M.: The Little Ice Age in Iberian mountains, *Earth-Science*
855 *Reviews*, 177, 175-208, [10.1016/j.earscirev.2017.11.010](https://doi.org/10.1016/j.earscirev.2017.11.010), 2018.
- 856 Painter, T. H., Flanner, M. G., Kaser, G., Marzeion, B., VanCuren, R. A., and Abdalati,
857 W.: End of the Little Ice Age in the Alps forced by industrial black carbon,
858 *Proceedings of the National Academy of Sciences*, 110, 15216-15221,
859 [10.1073/pnas.1302570110](https://doi.org/10.1073/pnas.1302570110), 2013.
- 860 Pauli, H., Gottfried, M., Dullinger, S., Abdaladze, O., Akhalkatsi, M., Alonso, J. L. B.,
861 Coldea, G., Dick, J., Erschbamer, B., Calzado, R. F., Ghosn, D., Holten, J. I., Kanka,
862 R., Kazakis, G., Kollár, J., Larsson, P., Moiseev, P., Moiseev, D., Molau, U., Mesa, J.
863 M., Nagy, L., Pelino, G., Puşcaş, M., Rossi, G., Stanisci, A., Syverhuset, A. O.,
864 Theurillat, J.-P., Tomaselli, M., Unterluggauer, P., Villar, L., Vittoz, P., and Grabherr,
865 G.: Recent Plant Diversity Changes on Europe's Mountain Summits, *Science*, 336,
866 353-355, [10.1126/science.1219033](https://doi.org/10.1126/science.1219033), 2012.
- 867 Pulido-Villena, E., Reche, I., and Morales-Baquero, R.: Food web reliance on
868 allochthonous carbon in two high mountain lakes with contrasting catchments: a stable
869 isotope approach, *Canadian Journal of Fisheries and Aquatic Sciences*, 62, 2640–2648
870 2005.
- 871 Ramos-Román, M. J., Jiménez-Moreno, G., R.S., A., García-Alix, A., Toney, J. L.,
872 Jiménez-Espejo, F. J., and Carrión, J. S.: Centennial-scale vegetation and North
873 Atlantic Oscillation changes during the Late Holocene in the southern Iberia,
874 *Quaternary Science Reviews*, 143, 84-95, 2016.
- 875 Rampen, S. W., Willmott, V., Kim, J.-H., Uliana, E., Mollenhauer, G., Schefuß, E.,
876 Sinninghe Damsté, J. S., and Schouten, S.: Long chain 1,13- and 1,15-diols as a
877 potential proxy for palaeotemperature reconstruction, *Geochimica et Cosmochimica*
878 *Acta*, 84, 204-216, <https://doi.org/10.1016/j.gca.2012.01.024>, 2012.
- 879 Rampen, S. W., Datema, M., Rodrigo-Gámiz, M., Schouten, S., Reichart, G.-J., and
880 Sinninghe Damsté, J. S.: Sources and proxy potential of long chain alkyl diols in
881 lacustrine environments, *Geochimica et Cosmochimica Acta*, 144, 59-71,
882 <http://dx.doi.org/10.1016/j.gca.2014.08.033>, 2014a.
- 883 Rampen, S. W., Willmott, V., Kim, J.-H., Rodrigo-Gámiz, M., Uliana, E., Mollenhauer,
884 G., Schefuß, E., Sinninghe Damsté, J. S., and Schouten, S.: Evaluation of long chain
885 1,14-alkyl diols in marine sediments as indicators for upwelling and temperature,
886 *Organic Geochemistry*, 76, 39-47, <https://doi.org/10.1016/j.orggeochem.2014.07.012>,
887 2014b.



- 888 Reche, I., Ortega-Retuerta, E., Romera, O., Pulido-Villena, E., Morales-Baquero, R., and
889 Casamayor, E. O.: Effect of Saharan dust inputs on bacterial activity and community
890 composition in Mediterranean lakes and reservoirs, *Limnol. Oceanogr.*, 54, 869–879,
891 2009.
- 892 Reimer, P. J., Bard, E., Bayliss, A., Beck, J. W., Blackwell, P. G., Ramsey, C. B., Buck,
893 C. E., Cheng, H., Edwards, R. L., Friedrich, M., Grootes, P. M., Guilderson, T. P.,
894 Haflidason, H., Hajdas, I., Hatté, C., Heaton, T. J., Hoffmann, D. L., Hogg, A. G.,
895 Hughen, K. A., Kaiser, K. F., Kromer, B., Manning, S. W., Niu, M., Reimer, R. W.,
896 Richards, D. A., Scott, E. M., Southon, J. R., Staff, R. A., Turney, C. S. M., and van
897 der Plicht, J.: IntCal13 and Marine13 Radiocarbon Age Calibration Curves 0–50,000
898 Years cal BP, *Radiocarbon*, 55, 1869–1887,
899 https://doi.org/10.2458/azu_js_rc.55.16947, 2013.
- 900 Rodrigo, F. S., Esteban-Parra, M. J., Pozo-Vázquez, D., and Castro-Díez, Y.: A 500-year
901 precipitation record in Southern Spain, *International Journal of Climatology*, 19, 1233–
902 1253, 10.1002/(SICI)1097-0088(199909)19:11<1233::AID-JOC413>3.0.CO;2-L,
903 1999.
- 904 Rodrigo-Gámiz, M., Martínez-Ruiz, F., Rampen, S. W., Schouten, S., and Sinninghe
905 Damsté, J. S.: Sea surface temperature variations in the western Mediterranean Sea
906 over the last 20 kyr: A dual-organic proxy (UK'37 and LDI) approach,
907 *Paleoceanography*, 29, 87–98, doi:10.1002/2013PA002466, 2014.
- 908 Rodrigo-Gámiz, M., Rampen, S. W., de Haas, H., Baas, M., Schouten, S., and Sinninghe
909 Damsté, J. S.: Constraints on the applicability of the organic temperature proxies
910 UK'37, TEX86 and LDI in the subpolar region around Iceland, *Biogeosciences*, 12,
911 6573–6590, 10.5194/bg-12-6573-2015, 2015.
- 912 Romero-Viana, L., Kienel, U., and Sachse, D.: Lipid biomarker signatures in a
913 hypersaline lake on Isabel Island (Eastern Pacific) as a proxy for past rainfall anomaly
914 (1942–2006AD), *Palaeogeography, Palaeoclimatology, Palaeoecology*, 350–352, 49–
915 61, <https://doi.org/10.1016/j.palaeo.2012.06.011>, 2012.
- 916 Sánchez-Castillo, P. M.: Algas de las lagunas de alta montaña de Sierra Nevada (Granada,
917 España), *Acta Botánica Malacitana*, 13, 21–52, 1988.
- 918 Sánchez-López, G., Hernández, A., Pla-Rabes, S., Trigo, R. M., Toro, M., Granados, I.,
919 Sáez, A., Masqué, P., Pueyo, J. J., Rubio-Inglés, M. J., and Giralt, S.: Climate
920 reconstruction for the last two millennia in central Iberia: The role of East Atlantic
921 (EA), North Atlantic Oscillation (NAO) and their interplay over the Iberian Peninsula,



- 922 Quaternary Science Reviews, 149, 135-150,
923 <https://doi.org/10.1016/j.quascirev.2016.07.021>, 2016.
- 924 Schmidt, G. A., Jungclauss, J. H., Ammann, C. M., Bard, E., Braconnot, P., Crowley, T.
925 J., Delaygue, G., Joos, F., Krivova, N. A., Muscheler, R., Otto-Bliesner, B. L.,
926 Pongratz, J., Shindell, D. T., Solanki, S. K., Steinhilber, F., and Vieira, L. E. A.:
927 Climate forcing reconstructions for use in PMIP simulations of the last millennium
928 (v1.0), *Geosci. Model Dev.*, 4, 33-45, [10.5194/gmd-4-33-2011](https://doi.org/10.5194/gmd-4-33-2011), 2011.
- 929 Schröter, D., Cramer, W., Leemans, R., Prentice, I. C., Araújo, M. B., Arnell, N. W.,
930 Bondeau, A., Bugmann, H., Carter, T. R., Gracia, C. A., de la Vega-Leinert, A. C.,
931 Erhard, M., Ewert, F., Glendining, M., House, J. I., Kankaanpää, S., Klein, R. J. T.,
932 Lavorel, S., Lindner, M., Metzger, M. J., Meyer, J., Mitchell, T. D., Reginster, I.,
933 Rounsevell, M., Sabaté, S., Sitch, S., Smith, B., Smith, J., Smith, P., Sykes, M. T.,
934 Thonicke, K., Thuiller, W., Tuck, G., Zaehle, S., and Zierl, B.: Ecosystem Service
935 Supply and Vulnerability to Global Change in Europe, *Science*, 310, 1333-1337,
936 <https://doi.org/10.1126/science.1115233>, 2005.
- 937 Shimokawara, M., Nishimura, M., Matsuda, T., Akiyama, N., and Kawai, T.: Bound
938 forms, compositional features, major sources and diagenesis of long chain, alkyl mid-
939 chain diols in Lake Baikal sediments over the past 28,000 years, *Organic*
940 *Geochemistry*, 41, 753-766, <https://doi.org/10.1016/j.orggeochem.2010.05.013>, 2010.
- 941 Sicre, M.-A., Jalali, B., Martrat, B., Schmidt, S., Bassetti, M.-A., and Kallel, N.: Sea
942 surface temperature variability in the North Western Mediterranean Sea (Gulf of Lion)
943 during the Common Era, *Earth and Planetary Science Letters*, 456, 124-133,
944 <https://doi.org/10.1016/j.epsl.2016.09.032>, 2016.
- 945 Sigl, M., Winstrup, M., McConnell, J. R., Welten, K. C., Plunkett, G., Ludlow, F.,
946 Buntgen, U., Caffee, M., Chellman, N., Dahl-Jensen, D., Fischer, H., Kipfstuhl, S.,
947 Kostick, C., Maselli, O. J., Mekhaldi, F., Mulvaney, R., Muscheler, R., Pasteris, D. R.,
948 Pilcher, J. R., Salzer, M., Schupbach, S., Steffensen, J. P., Vinther, B. M., and
949 Woodruff, T. E.: Timing and climate forcing of volcanic eruptions for the past 2,500
950 years, *Nature*, 523, 543-549, [10.1038/nature14565](https://doi.org/10.1038/nature14565)
951 [http://www.nature.com/nature/journal/v523/n7562/abs/nature14565.html#supplementar](http://www.nature.com/nature/journal/v523/n7562/abs/nature14565.html#supplementary-information)
952 [y-information](http://www.nature.com/nature/journal/v523/n7562/abs/nature14565.html#supplementary-information), 2015.
- 953 Steinhilber, F., Beer, J., and Fröhlich, C.: Total solar irradiance during the Holocene,
954 *Geophysical Research Letters*, 36, [10.1029/2009GL040142](https://doi.org/10.1029/2009GL040142), 2009.

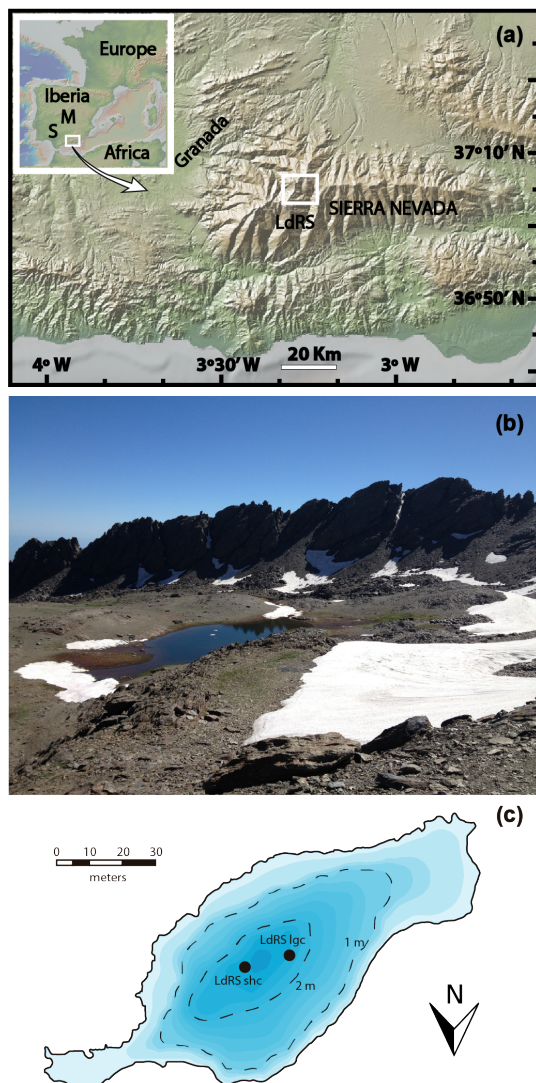


- 955 Stuiver, M., and Quay, P. D.: Changes in Atmospheric Carbon-14 Attributed to a Variable
956 Sun, *Science*, 207, 11-19, [10.1126/science.207.4426.11](https://doi.org/10.1126/science.207.4426.11), 1980.
- 957 Tejedor, E., Saz, M. Á., Cuadrat, J. M., Esper, J., and de Luis, M.: Temperature variability
958 in the Iberian Range since 1602 inferred from tree-ring records, *Clim. Past*, 13, 93-
959 105, [10.5194/cp-13-93-2017](https://doi.org/10.5194/cp-13-93-2017), 2017.
- 960 Theroux, S., D'Andrea, W. J., Toney, J., Amaral-Zettler, L., and Huang, Y.: Phylogenetic
961 diversity and evolutionary relatedness of alkenone-producing haptophyte algae in
962 lakes: Implications for continental paleotemperature reconstructions, *Earth and
963 Planetary Science Letters*, 300, 311-320, [10.1016/j.epsl.2010.10.009](https://doi.org/10.1016/j.epsl.2010.10.009), 2010.
- 964 Trouet, V., Esper, J., Graham, N. E., Baker, A., Scourse, J. D., and Frank, D. C.: Persistent
965 Positive North Atlantic Oscillation Mode Dominated the Medieval Climate Anomaly,
966 *Science*, 324, 78-80, [10.1126/science.1166349](https://doi.org/10.1126/science.1166349), 2009.
- 967 Versteegh, G. J. M., Bosch, H. J., and De Leeuw, J. W.: Potential palaeoenvironmental
968 information of C24 to C36 mid-chain diols, keto-ols and mid-chain hydroxy fatty
969 acids; a critical review, *Organic Geochemistry*, 27, 1-13,
970 [http://dx.doi.org/10.1016/S0146-6380\(97\)00063-6](http://dx.doi.org/10.1016/S0146-6380(97)00063-6), 1997.
- 971 Villanueva, L., Besseling, M., Rodrigo-Gámiz, M., Rampen, S. W., Verschuren, D., and
972 Sinninghe Damsté, J. S.: Potential biological sources of long chain alkyl diols in a
973 lacustrine system, *Organic Geochemistry*, 68, 27-30,
974 <http://dx.doi.org/10.1016/j.orggeochem.2014.01.001>, 2014.
- 975 Volkman, J. K., Barrett, S. M., and Blackburn, S. I.: Eustigmatophyte microalgae are
976 potential sources of C29 sterols, C22–C28 n-alcohols and C28–C32 n-alkyl diols in
977 freshwater environments, *Organic Geochemistry*, 30, 307-318,
978 [http://dx.doi.org/10.1016/S0146-6380\(99\)00009-1](http://dx.doi.org/10.1016/S0146-6380(99)00009-1), 1999.
- 979 Waters, C. N., Zalasiewicz, J., Summerhayes, C., Barnosky, A. D., Poirier, C., Gałuszka,
980 A., Cearreta, A., Edgeworth, M., Ellis, E. C., Ellis, M., Jeandel, C., Leinfelder, R.,
981 McNeill, J. R., Richter, D. d., Steffen, W., Syvitski, J., Vidas, D., Wagreich, M.,
982 Williams, M., Zhisheng, A., Grinevald, J., Odada, E., Oreskes, N., and Wolfe, A. P.:
983 The Anthropocene is functionally and stratigraphically distinct from the Holocene,
984 *Science*, 351, [10.1126/science.aad2622](https://doi.org/10.1126/science.aad2622), 2016.
- 985



986 **FIGURES**

987

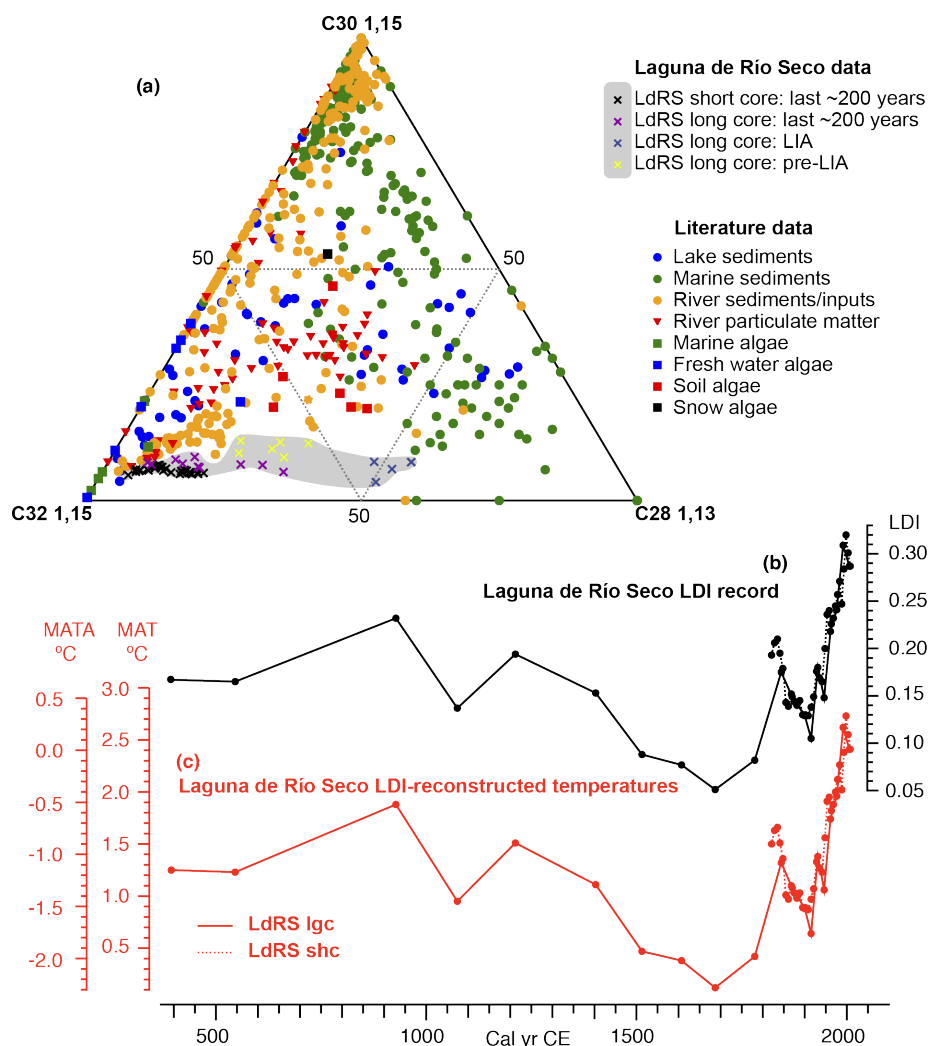


988

989 **Figure 1. Geographical setting.** (a) Location of the Sierra Nevada in the western
990 Mediterranean region, Madrid (M), Sevilla (S) and Granada observatories, as well as the
991 studied area: Laguna de Río Seco (LdRS), (b) LdRS catchment basin (0.42 ha) in spring
992 2013, (c) bathymetry map of LdRS along with the sampling points of both cores. Data
993 source and software: (a) map created by A. García-Alix using GeoMapApp (3.6.6)



994 (<http://www.geomapapp.org>), **(b)** picture from A. García-Alix, **(c)** digitalized map of a
995 bathymetry report from Egmasa S.A.
996



997

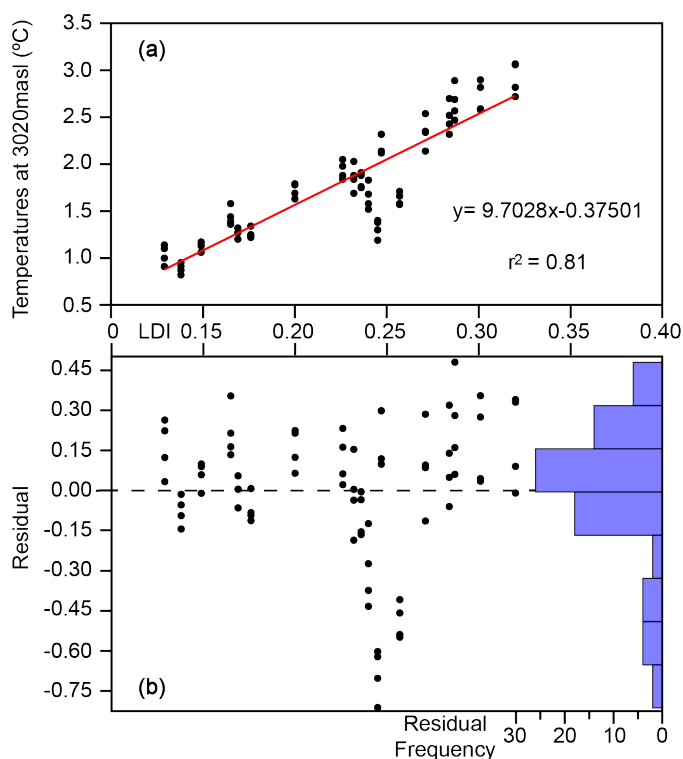
998 **Figure 2.** (a) Ternary diagram of the relative abundances of C₂₈ 1,13-diol, C₃₀ 1,15-diol
999 and C₃₂ 1,15-diol from LdRS short core (LdRS shc ~200 years) and LdRS long core
1000 (LdRS lgc ~1,500 years). Diol data compiled from the literature: lake sediments (Rampen
1001 et al., 2014a), algal cultures (Rampen et al., 2014a), marine sediments (Rampen et al.,
1002 2012; Rampen et al., 2014b; de Bar et al., 2016; Lattaud et al., 2017a), river
1003 sediments/inputs (de Bar et al., 2016; Lattaud et al., 2017b) (Lattaud et al., 2018), river
1004 particulate organic matter (Lattaud et al., 2018), (b) LDI record from LdRS, including



1005 both long core (line) and short core (dashed line), (c) Mean Annual Temperature (MAT
1006 °C) reconstruction from LDI records of LdRS, as well as Mean Annual Temperature
1007 Anomaly reconstruction (MATA °C) respect to the mean annual temperatures of the last
1008 30 years (2008-1979). Long core (line), short core (dashed line).
1009



1010

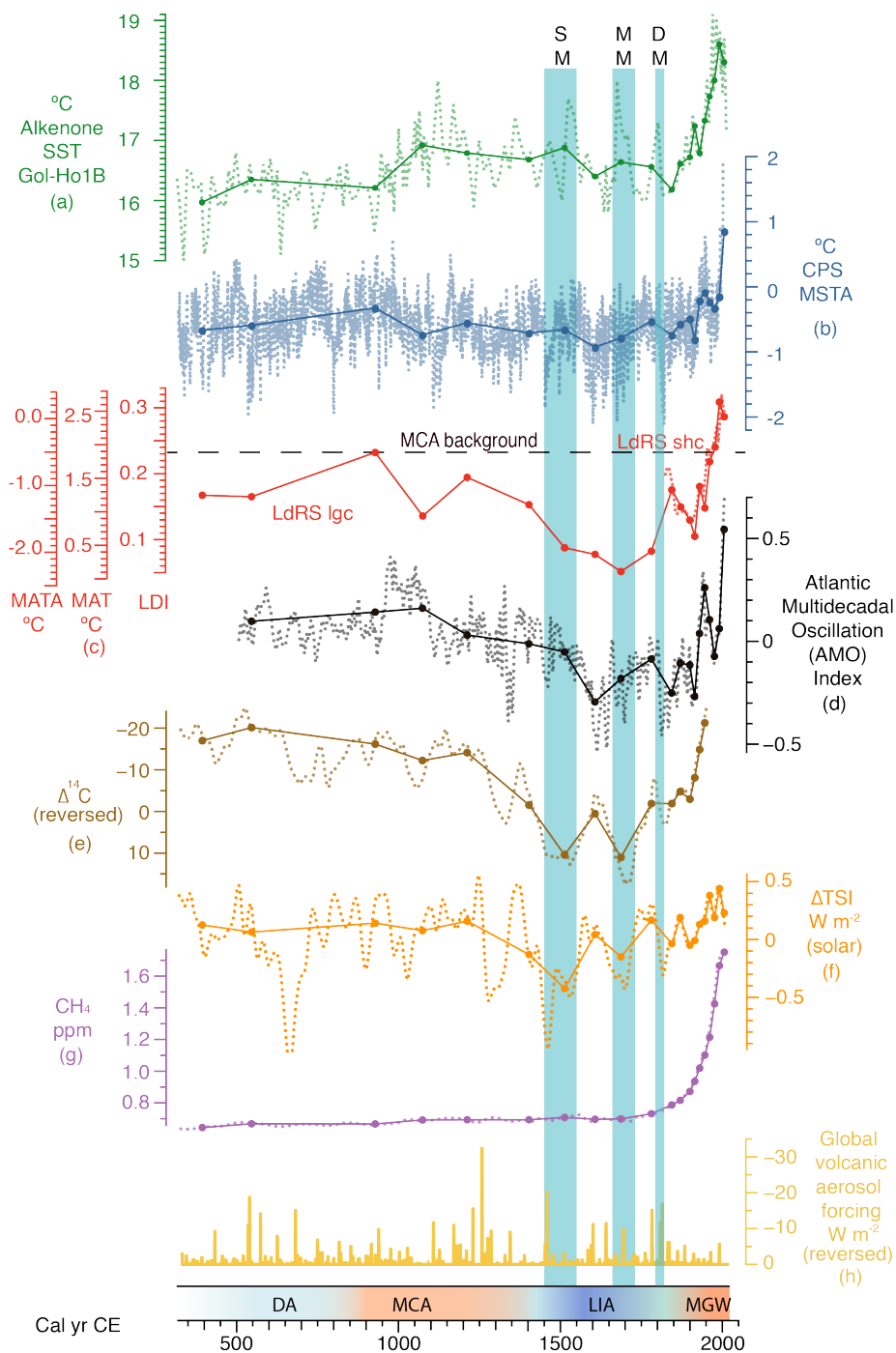


1011

1012 **Figure 3. LDI temperature calibration.** (a) Correlations by means of Ordinary Least
1013 Square regression between the LDI records from LdRS and the two groups of estimated
1014 temperature time-series at 3020 masl: Group 1) Temperatures obtained after correcting
1015 the instrumental temperature time-series from Madrid and Sevilla for the last ~100 years
1016 with the environmental lapse rate between low elevation and Sierra Nevada observatories
1017 (Spanish National Weather Agency - AEMet Open Data, 2019;Gonzalez-Hidalgo et al.,
1018 2015;Observatorio del cambio global de Sierra Nevada, 2016) (Table S4). Group 2)
1019 Temperatures obtained by means of the direct correlation among Madrid and Sevilla
1020 temperatures and those from the observatory Cetursa 5 at 3020 masl (Spanish National
1021 Weather Agency - AEMet Open Data, 2019;Gonzalez-Hidalgo et al., 2015;Observatorio
1022 del cambio global de Sierra Nevada, 2016) (Fig. S2), and (b) LDI values of LdRS vs.



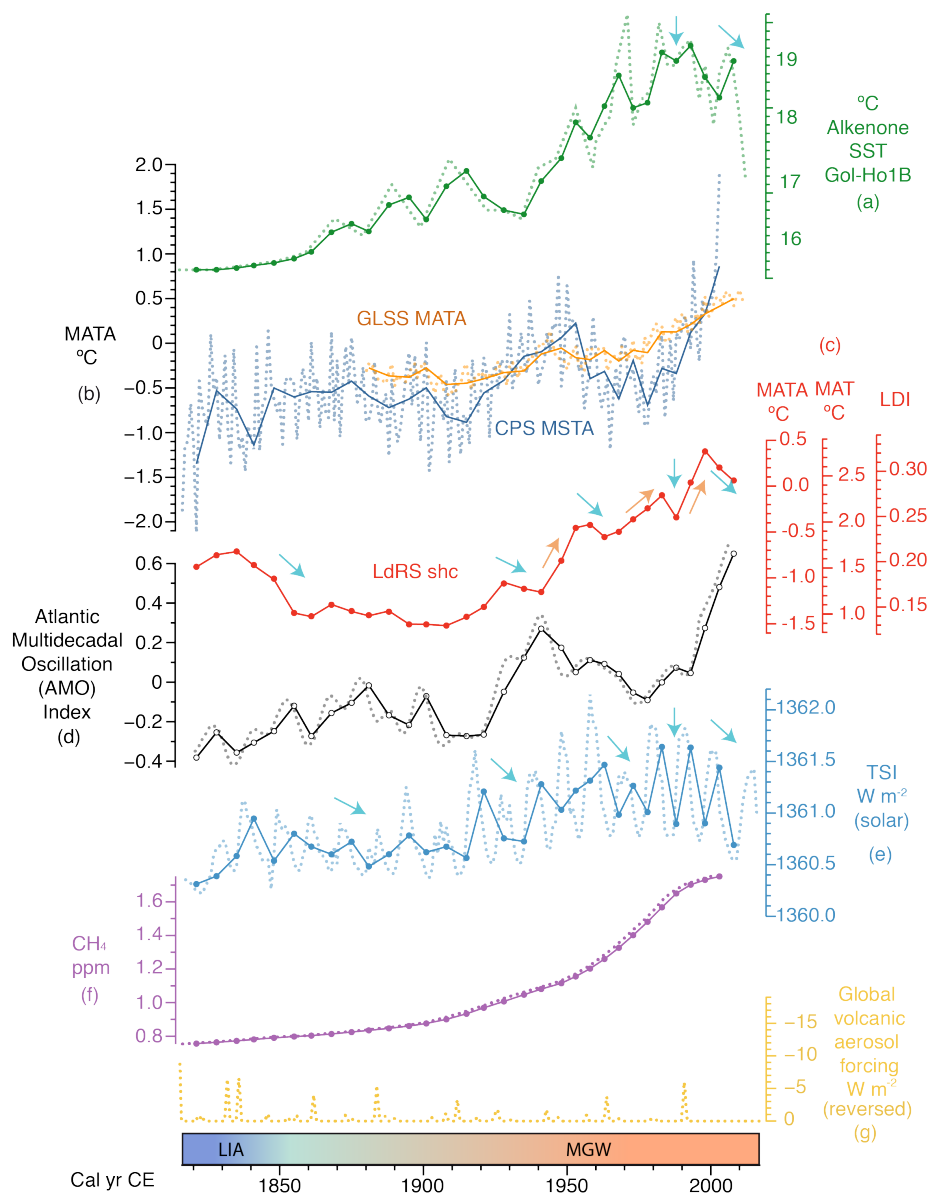
1023 residual temperatures (calculated between the calibrated LDI temperatures vs. reference
1024 temperature time series at 3020 masl), as well as the histogram of the frequency of these
1025 residuals.



1026



1027 **Figure 4. Comparison of the LDI and the reconstructed temperature record for the**
1028 **last ~1500 years of LdRS with temperature records, greenhouse gases, solar**
1029 **radiation and volcanic eruption records.** Original data are in dashed lines. Solid dots
1030 represent the same time averaging as the LDI data in LdRS lgc (data were linearly
1031 interpolated to the same resolution as the sampling points of LdRS lgc) to facilitate the
1032 Pearson correlation: **(a)** Alkenone-Sea Surface Temperatures (SST, °C) of the core Gol-
1033 Ho1B_KSGC-31 (Gulf of Lion: NW Mediterranean Sea (Sicre et al., 2016)), **(b)**
1034 Composite-plus-scaling (CPS) mean summer temperature anomaly reconstruction from
1035 tree rings records in Europe with respect to 1974-2003 CE (MSTA °C) (Luterbacher et
1036 al., 2016), **(c)** LDI record along with reconstructed mean annual temperatures (MAT °C)
1037 and mean annual temperature anomalies with respect to 1979-2008 CE (MATA °C) for
1038 the last 1500 years in LdRS (LdRS lgc, Laguna de Río Seco long core; LdRS shc, Laguna
1039 de Río Seco short core), **(d)** Atlantic Multidecadal Oscillation (AMO) reconstruction
1040 (Mann et al., 2009), **(e)** $\Delta^{14}\text{C}$ in the atmosphere (reversed) (Reimer et al., 2013), **(f)**
1041 reconstruction of the difference of the total solar irradiance from the value of the PMOD
1042 composite series during the solar cycle minimum of the year 1986 CE (1365.57 W m^{-2})
1043 (ΔTSI) (Steinhilber et al., 2009), **(g)** reconstructed concentration of atmospheric CH_4
1044 (ppm) (Schmidt et al., 2011), and **(h)** reconstruction of the global volcanic aerosol forcing
1045 (W m^{-2}) (reversed) (Sigl et al., 2015). Acronyms: DA, Dark Ages; MCA, Medieval
1046 Climate Anomaly; LIA, Little Ice Age; MGW, Modern Global Warming. Blue bars show
1047 three low solar activity periods, the Spörer Minimum (SM), the Maunder Minimum
1048 (MM), and the Dalton Minimum (DM).
1049



1050

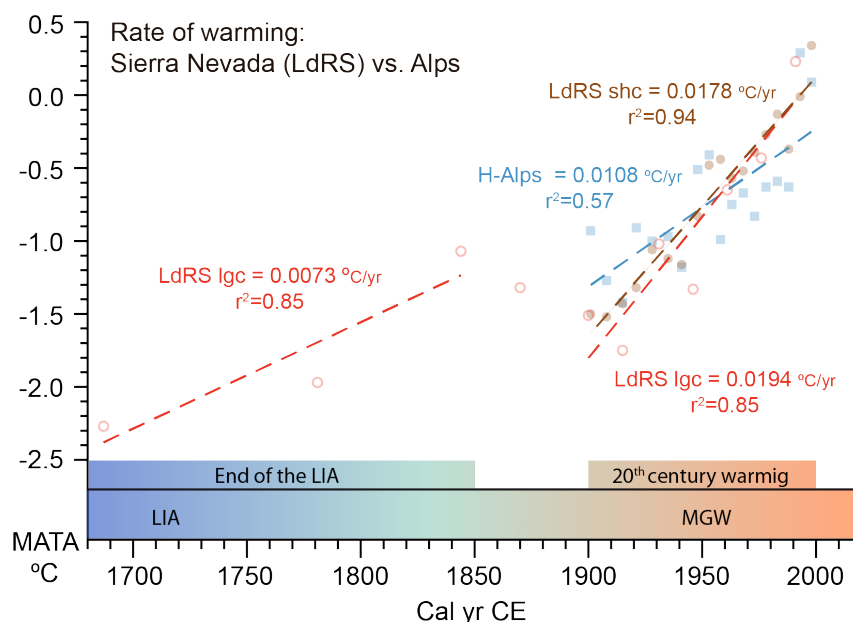
1051 **Figure 5. Comparison of the LDI and the reconstructed temperatures record for the**
 1052 **last ~200 years of LdRS with temperatures, greenhouse gases, solar radiation and**
 1053 **volcanic eruption records.** Original data are in dashed lines. Solid lines represent the
 1054 same time averaging as the LDI data in LdRS shc (data were linearly interpolated to the
 1055 same resolution as the sampling points of LdRS shc) to facilitate the Pearson correlation.



1056 (a) Alkenone-Sea Surface Temperatures (SST, °C) of the core Gol-Ho1B_KSGC-31
1057 (Gulf of Lion: NW Mediterranean Sea (Sicre et al., 2016)), (b) Composite-plus-scaling
1058 (CPS) mean summer temperature anomaly reconstruction from tree rings records in
1059 Europe with respect to 1974-2003 (MSTA °C) (Luterbacher et al., 2016) as well as global
1060 land and sea surface (GLSS) mean annual temperature anomalies with respect to 1979-
1061 2008 CE (MATA °C) (Hansen et al., 2010), (c) LDI record along with reconstructed mean
1062 annual temperatures (MAT °C) and mean annual temperature anomalies with respect to
1063 1979-2008 CE (MATA °C) for the last ~200 years in LdRS, (d) Atlantic Multidecadal
1064 Oscillation (AMO) reconstruction (Mann et al., 2009), (e) high resolution total solar
1065 irradiance reconstruction (TSI, $W m^{-2}$) (Coddington et al., 2016), (f) reconstructed
1066 concentration of atmospheric CH_4 (ppm) (Schmidt et al., 2011), and (g) reconstruction of
1067 the global volcanic aerosol forcing ($W m^{-2}$) (reversed) (Sigl et al., 2015). Acronyms: LIA,
1068 Little Ice Age; MGW, Modern Global Warming. Blue arrows: decrease; orange arrows:
1069 increase.
1070



1071



1072

1073 **Figure 6. Comparison between the average temperature warming rates from LdRS**

1074 **and the alpine areas of the Alps by means of Ordinary Least Square Regressions.**

1075 MATA (respect to the period 1979-2008 CE) from Laguna de Río Seco long core: LdRS

1076 lgc, red open circles, including the LIA and the 20th century; MATA for the 20th century

1077 (respect to the period 1979-2008 CE) from Laguna de Río Seco short core: LdRS shc,

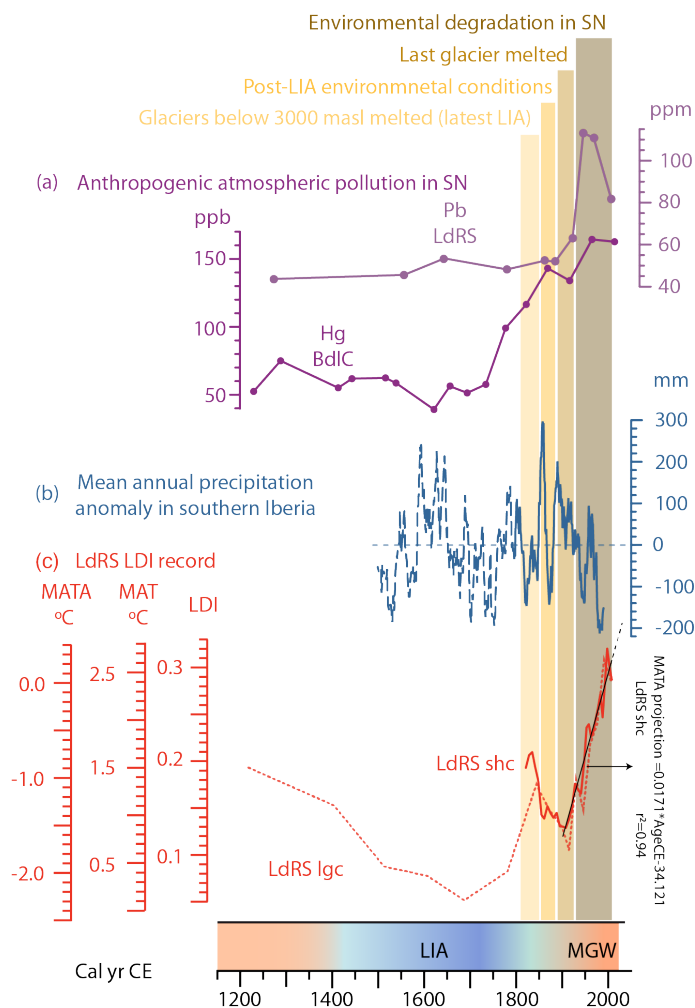
1078 brown closed circles; and high-Alps historical (homogenised) temperature records from

1079 the Historical Instrumental Climatological Surface Time Series of the Greater Alpine

1080 Region (HISTALP) database (Auer et al., 2007; Böhm et al., 2010) at the same time

1081 averaging as LdRS shc (data were linearly interpolated to the same resolution as the

1082 sampling points of LdRS shc) to facilitate the comparison (blue closed squares).



1083

1084 **Figure 7. Comparison among different factors affecting the environmental evolution**

1085 **of alpine wetlands in Sierra Nevada. (a)** records of anthropogenic heavy metal

1086 atmospheric pollution (Pb and Hg) in two alpine sites of Sierra Nevada: Laguna de Río

1087 Seco (LdRS) and Borreguil de la Caldera (BdlC) (Garcia-Alix et al., 2017; Garcia-Alix et

1088 al., 2013), **(b)** mean annual precipitation anomaly in southern Iberia from 1500 to 1990

1089 CE with respect to the mean value of the instrumental period (1791-1990 CE): solid line-

1090 instrumental data from Gibraltar, Southern Iberia, dashed line- anomaly precipitation

1091 reconstruction (Rodrigo et al., 1999), **(c)** LDI and temperature reconstruction in LdRS, as



1092 well as the MATA projection from an Ordinary Least Square Regression including LdRS
1093 she MATA for the last ~110 years (n=20). Colour bars indicate the four main
1094 environmental stages in the Sierra Nevada (SN) during the last 200 years. Acronyms:
1095 LIA, Little Ice Age; MGW, Modern Global Warming.